CHALMERS
UNIVERSITY OF TECHNOLOGY

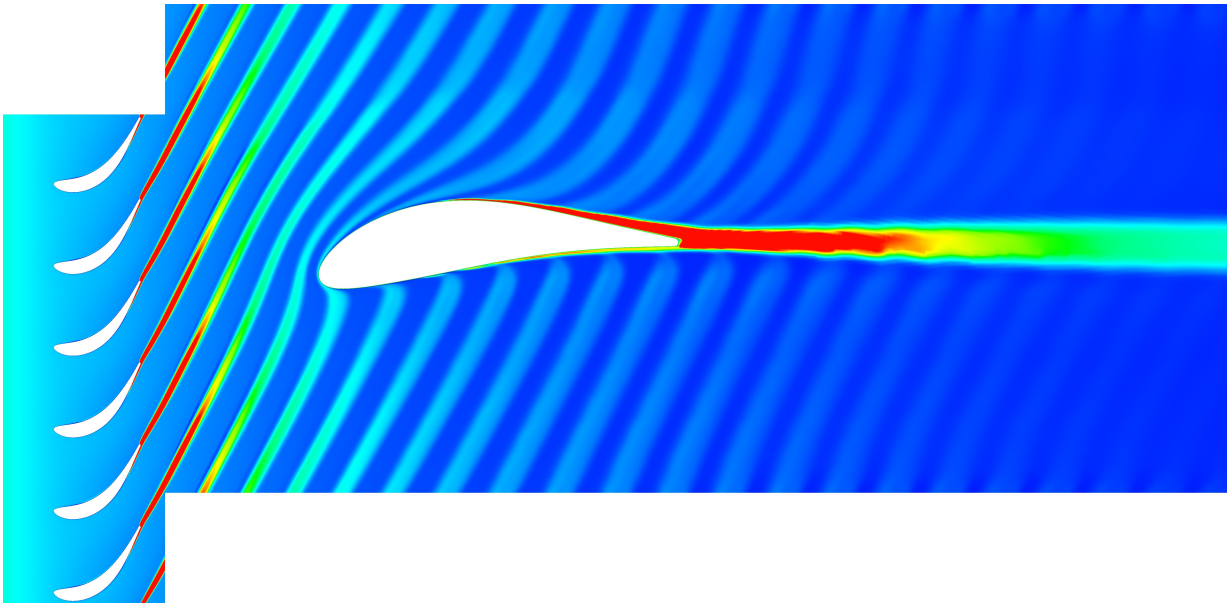

Unsteady LPT Blade Effects on Outlet Guide Vane Heat Transfer

Analysis of transient thermal loads induced by blade wakes in turbine rear structures

Master's thesis in Applied Mechanics

WILHELM DAHLIN

DEPARTMENT OF MECHANICS AND MARITIME SCIENCES

CHALMERS UNIVERSITY OF TECHNOLOGY
Gothenburg, Sweden 2025
www.chalmers.se

Master's thesis 2025

Unsteady LPT Blade Effects on Outlet Guide Vane Heat Transfer

Analysis of transient thermal loads induced by blade wakes in turbine rear structures

Wilhelm Dahlin

CHALMERS
UNIVERSITY OF TECHNOLOGY

Department of Mechanics and Maritime Sciences
Division of Fluid Mechanics
Chalmers University of Technology
Gothenburg, Sweden 2025

Unsteady LPT Blade Effects on Outlet Guide Vane Heat Transfer
WILHELM DAHLIN

Supervisor: Sravan Shakker, GKN Aerospace Sweden
Examiner: Tomas Grönstedt, Department of Mechanics and Maritime Sciences

Master's Thesis 2025
Department of Mechanics and Maritime Sciences
Division of Fluid Dynamics
Chalmers University of Technology
SE-412 96 Gothenburg
Telephone +46 31 772 1000

Cover: Taken from the 2D transient simulation results, a contour of the turbulence kinetic energy for the rotor and OGV domains.

Typeset in LaTeX
Printed by Chalmers Reproservice
Gothenburg, Sweden 2025

Unsteady LPT Blade Effects on Outlet Guide Vane Heat Transfer
WILHELM DAHLIN
Department of Mechanics and Maritime Sciences
Chalmers University of Technology

Abstract

Accurate thermal modeling in turbine rear structures (TRS) of aero-engines is crucial due to the high temperature air flow and cyclic thermal stresses induced by unsteady blade wakes from upstream low-pressure turbine (LPT) blades. Current industry practices predominantly rely on steady-state computational fluid dynamics (CFD) simulations to predict heat transfer coefficients (HTC). However, these models commonly underpredict HTC when compared to experimental measurements, primarily due to their inability to capture transient and unsteady effects.

In collaboration with GKN Aerospace Sweden, this thesis has focused on developing and analysing a two-dimensional transient CFD model of Outlet Guide Vane (OGV) heat transfer using sliding mesh techniques and advanced turbulence models, notably the SST-transition turbulence model. Validation of this model was conducted against experimental HTC data obtained from a 1.5-stage test rig at Chalmers. The transient simulations reveal clear periodic fluctuations in HTC due to the rotor blade wakes, phenomena inherently missed by steady-state models.

However, despite capturing temporal HTC variations and unsteady flow behaviour the transient CFD approach still resulted in HTC underpredictions compared to experimental data as well as 2D and 3D steady-state CFD models. This discrepancy is attributed not only to limitations inherent in two-dimensional modeling but also to the need for more advanced turbulence modeling and potential inaccuracies stemming from an outdated mesh study based on incorrect boundary conditions. The study suggests further research should focus on resolving these issues through refined turbulence modeling strategies, accurate boundary condition implementation, and rigorous mesh studies to enhance predictive accuracy as well as industrial relevance and applicability.

Keywords: heat transfer, convection, heat transfer coefficient (HTC), computational fluid dynamics (CFD), transient, turbine rear structure (TRS), outlet guide vane (OGV), turbulence, transition.

Acknowledgements

This thesis marks the end of an exciting journey and my first steps into the aerospace industry. It has been an intense period of learning, growth, and occasional head-scratching moments - but most of all, a time filled with the support of many kind, knowledgeable and generous people.

I would especially like to thank the thermal team at GKN: Sravan Shakker, Aravind Murali, and Hans Abrahamsson. Your support, positivity, and patience (even when things didn't go quite as planned) made this project not only possible but truly enjoyable. I couldn't have asked for a better team to learn from.

I would also like to thank Tomas Grönstedt, my examiner, for his thoughtful feedback and assistance throughout this work. Finally, to everyone else at GKN and Chalmers who took the time to answer my many questions, share your experience, and make me feel welcome - thank you.

Wilhelm Dahlin, Gothenburg, June 2025

List of Acronyms

Below is the list of acronyms that have been used throughout this thesis listed in alphabetical order:

OGV	Outlet Guide Vane
TRS	Turbine Rear Structure
LPT	Low Pressure Turbine
PS	Pressure Side
SS	Suction Side
CFD	Computational Fluid Dynamics
RANS	Reynolds Averaged Navier-Stokes
URANS	Unsteady RANS
BC	Boundary Condition
HTC	Heat Transfer Coefficient
CTR	Chalmers Test Rig
IRT	Infrared Thermography
CAD	Computer Aided Design
TA	Time-Averaged
Avg	Average

Nomenclature

Below is the nomenclature of indices, parameters, and variables that have been used throughout this thesis.

Indices

i,j,k	Indices for x-,y- and z-coordinates, respectively
∞	free-stream
s	Surface
b	Bulk

Parameters

k_{cond}	Thermal conductivity
ε	emissivity
h	Heat transfer coefficient (HTC)
ρ	Density
ν	Kinematic viscosity
μ	Dynamic viscosity
μ_t	Eddy viscosity
θ	Momentum thickness
c_p	Specific heat capacity
α	Thermal diffusivity

Variables

ϕ	Flow coefficient
t	time

q	Heat flux
u	velocity
U	Mean velocity
u_τ	Friction velocity
ω	angular velocity
T	Temperature
p	Pressure
τ_w	Wall shear stress
k	Turbulence kinetic energy
ε	Eddy dissipation rate
ω	Specific dissipation rate
I	Turbulence intensity
L	Turbulence length scale
P	Production terms
γ	Intermittency
Re_θ	Onset momentum thickness Reynolds number

Constants

σ	Stefan-Boltzmann constant
C_μ	Constant used for turbulence modeling in ANSYS Fluent
$\alpha, \beta, \beta^*, \sigma_k, \sigma_\omega$	Constants used in $k-\omega$ turbulence model

Contents

List of Figures

List of Tables

1
Introduction

This thesis investigates the unsteady thermal effects induced by blade wakes on the Outlet Guide Vane within the turbine rear structure in an aero-engine. Conducted as part of the collaborative effort between Chalmers University of Technology and GKN Aerospace Sweden, this study involves developing CFD models which are validated against experimental data from a 1.5-stage LPT-OGV test rig at Chalmers. The main outcome is to provide insights into transient heat transfer phenomena, assisting GKN in enhancing the reliability and performance of turbine components.

1.1 Background

Efficient propulsion is essential for aircraft performance, relying on carefully designed engine components to manage factors such as thrust and airflow. One such component is the Turbine Rear Structure (TRS), positioned after the low pressure turbine (LPT) according to figure 1.1.

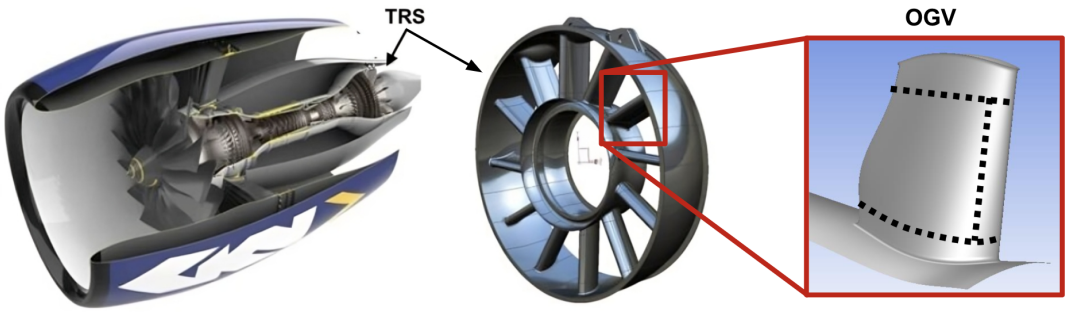

Figure 1.1: TRS Location in aero-engine (left), TRS housing the OGVs (middle) and one single OGV showing common weld locations (right).

The TRS provides structural support and is used to mount the engine to the aircraft body, while also facilitating other functions such as oil and purge flow. Additionally, the Outlet Guide Vanes (OGVs) are part of the TRS and helps de-swirl the hot exhaust, leading to a more axially directed flow thus reducing turbulence and improving overall efficiency. The OGVs are often welded to the end walls as can be seen in the figure above. Furthermore, modern aero-engines utilize higher and higher bypass ratios in order to increase performance and reduce engine noise. Depending on whether the turbofan is geared or ungeared, the requirements on the rotational speed of the LPT varies greatly. This leads to a large variance in the swirl angle out of the LPT, which puts great focus on designing robust OGVs that can handle large incidence variations.

The TRS is subjected to high-temperature flows of 600-700° C, which impose significant thermal gradients on the OGV, most prominently along the leading edge where the heat transfer coefficient (HTC) is at its highest. Although the flow temperature remains below the thermal limit of the OGV material, the repeated cycles of heating during operation and cooling in between cycles lead to continuous thermal expansion and contraction of the vane structure. The welding fillets do not expand and contract in perfect synchrony with the vane material due to differences in geometry, material properties, and local heat transfer conditions which leads to a mismatch in thermal response. This generates localized stresses that accumulate over time, leading to fatigue damage in the welds and contributing to overall structural wear. In order to evaluate the thermal behaviour and assess fatigue risk accurately, it is thus essential to have a reliable prediction of the HTC distribution along the OGV.

Today, GKN uses steady-state simulations when predicting thermal behaviour in the TRS. This data is validated against a test rig at Chalmers University of Technology (described in more detail under section 1.2). The current results shows that the steady CFD models underpredict the HTC magnitude and does not capture transitional behaviour accurately. This discrepancy is not unexpected since steady simulation models are not able to capture the unsteady nature and natural flow characteristics of the problem.

According to previous studies, the HTC at the stagnation point of a cylinder in cross flow can increase by up to 50 percent when under the influence of higher turbulence levels (described further in section 1.3). In order to improve the accuracy of the current CFD models used for predicting the HTC in the TRS, GKN wishes to evaluate the validity of transient simulation models, starting with a 2D model to reduce overall computational cost. This will give more insight as to how the flow behaves in the TRS and should in theory yield more accurate predictions of the HTC compared to the steady models.

1.2 The 1.5-Stage LPT-OGV Test Rig at Chalmers

As part of the collaboration between Chalmers and GKN, a 1.5-stage test rig was developed and is used for various measurements, both aerodynamic and thermal [2]. The geometry of the turbomachinery components were developed by GKN. It being a 1.5-stage configuration simply refers to the fact that there is one LPT vane, one rotor and one OGV - equating to one-and-a-half stages. The geometry was developed by GKN. A schematic view of the full setup along with a CAD-model showing the 1.5-stage geometry can be seen in figure 1.2.

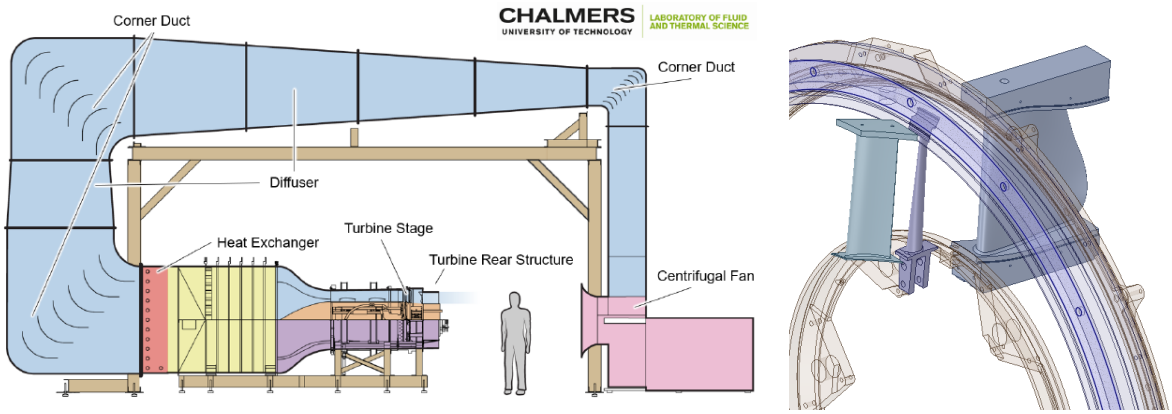

Figure 1.2: Schematic view of the Chalmers test rig (left) and the 1.5-stage geometry from GKN (right).

As illustrated above, ambient air is drawn into the system by a centrifugal fan (shown in pink). The flow is then guided through a series of corner ducts (shown in blue) and directed toward the heat exchanger (shown in red), where it is adjusted to the desired inlet temperature. Downstream of the heat exchanger, several flow-conditioning grids with varying geometries are installed to minimize large-scale flow disturbances (shown in yellow). The flow then continues through the diffuser and enters the turbine stage, followed by the TRS (including the OGVs). After passing through the TRS, the air is let back out into the surrounding environment. Various probes and sensors can be mounted at different radial and tangential positions upstream, within, and downstream of the OGV section. While the rig is operated using ambient conditions, it can still produce conditions representative of actual engine operation. This is discussed more under section 1.2.1

Referring to figure 1.3, there is one specially designed OGV (painted in black) which is equipped to allow for heat transfer measurements. The temperature on this OGV surface is measured using infrared thermography (IRT). It has internal water channels which provide warm water circulation to heat the vane, which together with the cooler airflow induces a heat flux. The surface of the OGV is covered with a high-emissivity and low-reflection coating to measure the surface temperature more accurately. Consequently, high-reflection gold leaf markers are attached to get a geometrical reference as well as allowing for measurements of background temperature. The reference temperatures were measured using resistance temperature detectors (RTDs). Finally, the heat transfer distribution is calculated by solving the three-dimensional conjugate heat transfer from OGV to airflow.

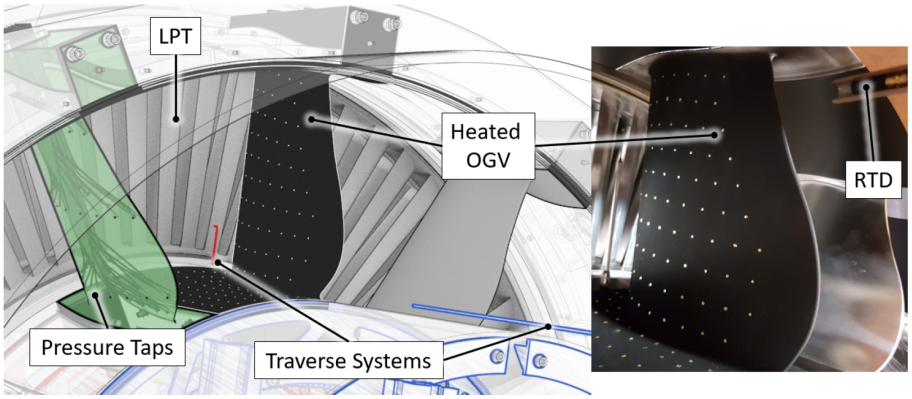

Figure 1.3: Schematic illustration of the test section (left) and photo of the OGV used for thermal measurements (right).

1.2.1 Operating Conditions in Real Applications vs Chalmers Test Rig

In real aero-engines, the TRS is subject to high temperatures and pressures, and at moderate to high subsonic speeds. In contrast, the CTR is operated using nearly ambient conditions and low flow speeds (M<0.3). While this varies greatly from the conditions during actual engine operation, factors such as the Reynolds number and flow coefficient is matched through appropriate scaling of blade speeds and dimensions. This ensures that the key non-dimensional parameters governing turbulence and heat transfer remain representative of engine-relevant conditions. This simplifies testing and instrumentation while still capturing relevant flow phenomena accurately and in a representative way.

1.2.2 Measurement Limitations

Due to the current setup of the test rig, there are some inherent limitations regarding different measurements. Firstly, pressure and velocity components cannot be measured at all locations of interest. For instance, this data is not available between the LPT vane and rotor. These quantities are instead taken from other CFD models (as discussed later in section 3.2)

Furthermore, the CTR does not allow for measurements along the OGV leading edge or aft-most section due to the inherent constraints of the rig setup and the given measurement technique. As can be seen in figure 1.4, the IR camera is placed outside the TRS and measures the OGV surface temperature through a small opening covered in plastic, as to not disturb the flow inside the rig. However, this setup limits the view of the whole OGV, such that leading edge and aft are hidden. This is a well-known limitation and improvements for upcoming test rigs are being considered.

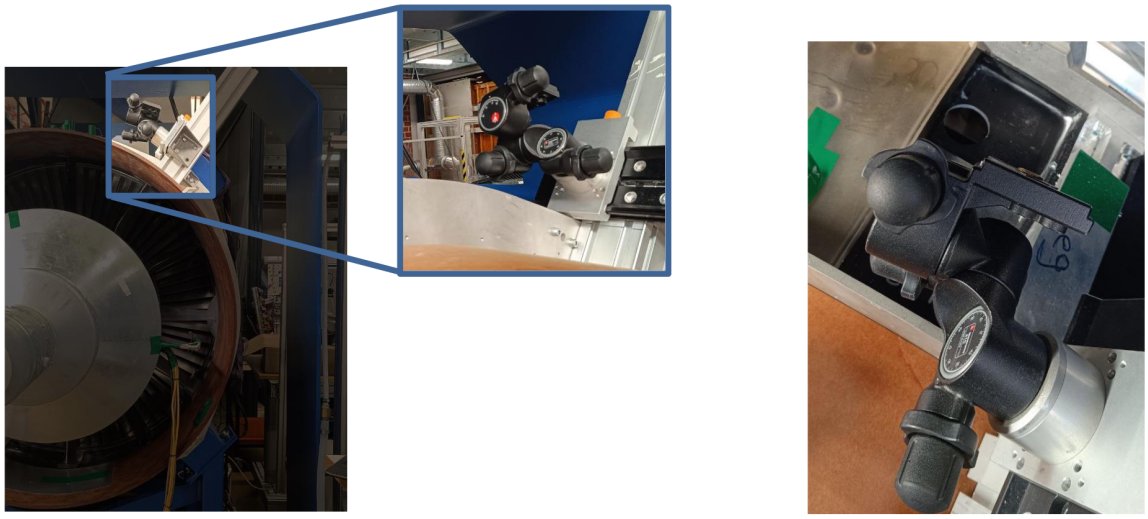

Figure 1.4: Position and close-up of the IR camera in the test rig (left) and the hole through which measurements are performed.

1.3 Previous Work and Literature Study

The understanding of heat transfer phenomena, turbulence modeling, and unsteady flow characteristics in turbomachinery applications has been significantly advanced through both experimental and numerical investigations. This section begins by examining foundational studies on turbulence effects and heat transfer, followed by reviewing relevant prior research conducted at GKN and Chalmers. Finally, attention is given to recent advances in transient modeling and unsteady flow dynamics, which are directly relevant to the simulation methods employed in this thesis.

1.3.1 General Studies on Turbulence and Heat Transfer

The influence of turbulence on HTC, particularly on cylindrical and similarly shaped geometries, has been widely studied due to its significance in thermal modeling of turbomachinery components.

Lowery and Vachon (1975) experimentally demonstrated that increased turbulence intensity substantially elevates the stagnation region HTC on heated cylinders up to 50 percent [3]. Their study established a direct correlation between turbulence characteristics and local heat transfer enhancements, providing foundational insights into turbulence-induced HTC variation.

Further extending these findings, Ames and Moffat (1990) conducted experiments detailing how large-scale, high-intensity turbulence significantly boosts heat transfer, especially in stagnation regions on cylindrical bodies [4]. These observations underscored the necessity of incorporating turbulence effects into heat transfer predictions, reinforcing the validity of transient and detailed turbulence modeling.

Wang and Vanka (1995) provided numerical evidence supporting experimental observations by confirming the strong sensitivity of HTC distribution to turbulence intensity and vortex shedding phenomena around cylinders [5]. Their computational insights form a critical reference for validating numerical methods and understanding flow-induced thermal dynamics.

Moreover, Scholten and Murray (1998) offered experimental evidence on the transient nature of HTC around cylinders subjected to cross-flow, emphasizing the impact of turbulence-driven fluctuations on instantaneous and time-averaged HTC values [6]. This study further underlines the importance of resolving turbulence accurately in transient simulations.

1.3.2 Previous Studies at GKN Aerospace and Chalmers

Several studies have been carried out at GKN and Chalmers focusing on the heat transfer characteristics of the TRS and OGV.

Murali (2023) conducted a thorough investigation into flow transition in the TRS and the accuracy of various turbulence models. Utilizing steady-state CFD simulations, Murali found found that while the transition-SST turbulence model captures transition effectively, the HTC predictions were consistently lower than experimental data from the CTR, possibly emphasizing the limitations inherent in steady-state approaches. In his work, Murali also compared HTC magnitudes and trends for empirical correlations (cylinders and flat plates) with the CFD results for the OGV. Using the OGV geometry generally exhibited similar HTC predictions as those from correlations, suggesting that other research using cylinders in cross flow is still representative of the current study where the TRS is investigated.

Dhanasegaran (2018) undertook extensive experimental and computational studies at Chalmers, focusing specifically on OGVs [8]. Employing IR measurement techniques alongside numerical methods (SST k-ω turbulence model), this research provided comprehensive validation of CFD models against experimental data, highlighting crucial heat transfer phenomena on OGV surfaces under realistic engine conditions.

Additionally, Wang et al. (2016) explored OGV heat transfer using thermochromic liquid crystals within a linear cascade test rig, assessing the effects of varying inlet flow angles on HTC [9]. The research highlighted boundary layer transition and separation as critical phenomena affecting local HTC values.

1.3.3 Transient and Swirling Flow Modeling

Yang et al. (2024) highlighted the critical role of accurately modeling transient performance and heat transfer effects within gas turbine engines [10]. Their comprehensive review stressed the need for improved simulation platforms capable of accurately capturing heat soakage, tip clearance effects, and transient flow behaviour.

In summary, the literature indicates a clear consensus on the importance of employing detailed transient simulations and advanced turbulence modeling techniques to capture the complexities of heat transfer phenomena in OGVs accurately. This thesis builds upon previous foundational research and utilizes validated computational strategies to enhance the understanding of transient HTC behavior under realistic operating conditions.

1.4 Aim and Objectives

A 2D transient CFD model will be developed to analyse the unsteady effects from upstream rotors on the HTC and flow transition along the OGV. This model will capture the temporal variations in flow behavior to provide a deeper understanding of turbulence-driven phenomena. Additionally, a 2D steady-state model will be created to serve as a reference for comparison with the transient simulations as well as with Murali's previous 3D steady-state simulation results. This comparison will help assess the reliability and accuracy of the different modeling approaches. Furthermore, the numerical results will be validated against experimental data obtained from the Chalmers test rig, ensuring that the models provide a realistic and accurate representation of physical flow behavior.

Finally, to ensure the correct representation of wake and turbulence structures, a comprehensive mesh resolution study will be conducted. This study will determine the necessary mesh requirements to accurately preserve upstream flow characteristics and prevent premature dissipation due to numerical diffusion.

In summary, the main objectives of this thesis are to:

- Develop a 2D transient CFD model to evaluate how unsteady effects from upstream rotors affect the HTC and transition on the OGV
- Develop a 2D steady model, used to compare with the transient model as well as previous 3D steady results
- Compare the HTC predictions of all CFD models as well as the experimental data from Chalmers
- Establish specific mesh resolution requirements needed in order to capture and maintain upstream waked and turbulent structures.

1.4.1 Limitations

Given the limited time frame and the need to keep computational demands within reasonable ranges, several simplifications were set. These were not only practical but also ensured that the study remained focused on the key objective of evaluating transient wake effects on OGV heat transfer.

- **Dimensional Reduction to 2D:** In order to enable transient analysis within reasonable computational limits, a two-dimensional model was used. While this approach omits certain three-dimensional flow structures, it allows detailed resolution of time-resolved wake effects and flow transition, which are central to this investigation.

- **Stator Exclusion:** The upstream stator (LPT vane) was excluded from the domain to reduce complexity and simulation time. Its influence is instead approximated through appropriate boundary conditions and inflow turbulence parameters derived from prior simulations and experimental data.
- **Geometric Simplification:** The model uses a midspan cross-section of the rotor blades and OGV. This simplification provides valuable insight into span-wise flow characteristics at this location but naturally excludes end wall effects and radial gradients.
- **2D Motion Representation:** As rotational effects cannot be directly modeled in 2D, a sliding mesh approach with periodic translational motion was employed. While an approximation, this method has been shown in literature to capture key unsteady wake transport mechanisms with sufficient accuracy.
- **CTR vs Engine Conditions:** Although the Chalmers Test Rig operates at near-ambient pressures and temperatures, Reynolds number and flow coefficient matching ensures engine-representative flow physics. Nevertheless, some thermophysical deviations are unavoidable.
- **Measurement Coverage:** The current experimental setup does not allow for full HTC mapping at the OGV leading edge or trailing edge. As a result, validation is limited to the mid-chord region, which must be considered when interpreting the model's predictive capabilities.

1.4.2 Areas of Investigation

The main objective of this thesis is to evaluate transient effects on the OGV heat transfer. The following research questions outline the key areas of investigation:

- How well do 2D steady-state models predict HTC on the OGV compared to 3D steady-state models?
- How are HTC predictions affected when implementing a 2D transient model as opposed to a 2D steady-state model?
- Is the 2D transient model results more accurate than the steady-state model when validating against the CTR experimental data?
- What are the mesh resolution requirements in order to capture the unsteady flow phenomena as well as the HTC?
- How is the HTC affected by varying inlet turbulence boundary conditions?

2

Theory

This chapter provides the theoretical background necessary to understand and interpret the heat transfer and flow phenomena observed in turbomachinery, specifically for the turbine rear structure. Fundamental concepts such as fluid dynamics, heat transfer mechanisms, turbulence modeling approaches, and characteristic turbomachinery parameters are discussed to establish a solid foundation for understanding the CFD methodologies and results presented in subsequent chapters.

2.1 Turbomachinery Fundamentals

Modern turbofan engines consist of multiple modules working together to compress air, extract energy, and generate thrust [11]. Referring to figure 2.1, ambient air is first drawn into the engine through the intake and passes through the fan. A portion of the air continues into the engine core, where it is compressed by a series of axial compressors to raise the pressure and temperature. After compression, the air enters the combustion chamber, where it is mixed with fuel and ignited. The resulting high-energy exhaust gases expand through multiple turbine stages, driving the upstream compressor and fan. The final turbine stage is followed by the Turbine Rear Structure (TRS), which includes the Outlet Guide Vanes (OGVs).

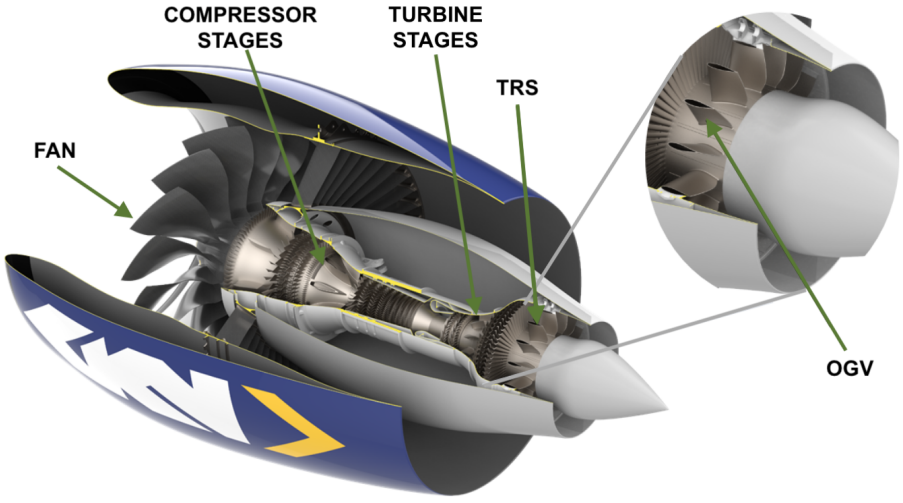

Figure 2.1: Cross-sectional view of a typical turbofan engine, showcasing its main components.

2.1.1 TRS Architecture and Function

The TRS is an structural component of the engine and is used to mount the engine to the aircraft body [12]. It can reach temperatures of 600-700° C during operation. The TRS also provides space and integration capability for systems such as purge flows, oil supply lines, and other essential engine components.

Furthermore, the OGVs assist with removing residual swirl from the flow and redirects it axially from the LPT toward the exhaust nozzle. While they are not load-bearing, they are typically welded onto the structural end walls. These welds are particularly susceptible to fatigue caused by the thermal cycling described under section 1.1, especially near the OGV leading edge, where heat transfer rates are most severe.

2.1.2 Characteristic Flow Features

Flow through turbomachinery, and particularly through the TRS, is influenced by a combination of geometrical constraints and unsteady interactions with upstream components [13]. Key characteristics include:

- **Swirling Flow:** The exhaust from the LPT rotor possesses significant tangential velocity. The OGVs must realign this flow to be predominantly axial.
- **Incidence Variation:** The angle at which flow impinges on the OGV varies with engine load, operating conditions (i.e. on- vs off-design), bypass ratio, and upstream stage behavior, particularly in geared versus ungeared turbofans.
- **Wake Interaction:** Flow is highly non-uniform due to upstream wake- and vortex shedding from the rotor blades. This induces turbulence and transition on the OGV surface.
- **Boundary Layer Effects:** Adverse pressure gradients can lead to separation, transition, or reattachment of the boundary layer, particularly on the suction side.

2.1.3 Parameters and Coefficients

Several geometric and flow-related parameters play a role in analysing turbomachinery flows:

- **Swirl Angle:** Angle between the absolute flow direction and the axial direction. It indicates how far from axial the flow is and is directly influenced by upstream rotor behavior.
- **Incidence Angle:** Angle between the incoming flow vector and the blade/vane leading edge. This angle strongly affects phenomena such as separation and local HTCs.
- **Flow Coefficient:** A non-dimensional quantity which describes how efficient the rotating components are at converting rotational motion to axial. It is defined as the ratio of the axial and tangential flow components (u_x and ω_r, respectively) and is given by

$$\phi = \frac{u_x}{\omega_r} \tag{2.1}$$

It is very commonly used to assess flow behavior through turbomachinery stages.

2.1.4 Heat Transfer in Turbomachinery

Heat transfer in turbine vanes is dominated by convection, with additional contributions from conduction within the material and radiation in high-temperature regions (however the two latter are not under investigation in this thesis). In the TRS, convective heat transfer is strongly affected by:

- **Turbulence and Transition:** Transition from laminar to turbulent flow significantly increases local HTC, particularly near the leading edge.
- **Wake Impact:** Upstream rotor wakes periodically impinge on the OGV surface, enhancing turbulence and unsteady thermal loading.
- **Surface Curvature and Geometry:** Leading edge curvature leads to stagnation heating, while trailing edge regions may experience separation and reduced HTC.

2.2 Heat Transfer Mechanisms

In thermal systems, energy can be transferred between materials or across boundaries via three primary mechanisms: conduction, convection, and radiation [14]. These mechanisms are governed by the first and second laws of thermodynamics and arise when a temperature gradient exists between two regions or materials.

In the present work, convective heat transfer dominates due to the interaction between the high-speed airflow and solid turbine surfaces. Nonetheless, conduction and radiation are briefly discussed for completeness and for their relevance to experimental data interpretation.

2.2.1 Conduction

Conduction occurs within solid materials when there is a temperature gradient. The rate of conductive heat transfer q''_{cond} can be expressed as:

$$q''_{\text{cond}} = -k_{\text{cond}} \frac{dT}{dx} \tag{2.2}$$

where k_{cond} is the thermal conductivity of the material and dT/dx is the temperature gradient in the direction of heat flow.

2.2.2 Radiation

Radiation involves the emission of electromagnetic energy from a surface. The radiative heat flux is given by the Stefan-Boltzmann law:

$$q''_{\text{rad}} = \varepsilon \sigma T^4 \tag{2.3}$$

where ε is the surface emissivity, σ is the Stefan-Boltzmann constant, and T is the absolute temperature. Radiation effects are small in this work but must be considered in the CTR when interpreting infrared thermography (IRT) measurements.

2.2.3 Convection

Convection is the dominant heat transfer mode in turbomachinery and involves heat transport between a solid surface and a moving fluid. It is driven by both molecular diffusion and bulk motion of the fluid. The convective heat transfer rate is described by:

$$q''_{\text{conv}} = h(T_s - T_b) \tag{2.4}$$

where h is the heat transfer coefficient (HTC), T_s is the surface temperature, and T_b is the bulk fluid temperature. Several factors influence convective heat transfer in turbomachinery:

- **Flow Velocity:** Higher velocities enhance mixing and disrupt the boundary layer, thus increasing the HTC.
- **Turbulence:** Turbulent flows also promote mixing and reduce the thickness of the thermal boundary layer.
- **Surface Roughness:** Increases turbulence and the effective surface area which in turn increases the HTC.
- **Thermal Properties:** Fluid viscosity, specific heat, and conductivity all influence convective behavior.

2.2.4 Conjugate Heat Transfer

Conjugate Heat Transfer (CHT) describes the simultaneous solution of heat transfer in both fluid and solid domains. It accounts for thermal conduction within the solid, convection at the surface, and any relevant radiation. Although not modeled directly in this work, CHT is important in interpreting experimental data and in real engine operation where internal conduction affects surface temperatures. This is taken into consideration in the test rig at Chalmers.

2.2.5 Effect of Turbulence on Heat Transfer

Turbulence significantly enhances convective heat transfer by increasing fluid mixing and reducing thermal boundary layer thickness. Elevated turbulence levels promote earlier transition from laminar to turbulent flow, leading to higher local HTCs. This phenomenon is especially pronounced at stagnation regions and leading edges, where turbulent fluctuations disrupt boundary layers. Turbulence parameters such as intensity, length scale, and eddy dissipation directly influence the predicted HTC in CFD simulations. Accurate representation of these parameters in turbulence modeling is critical for reliable predictions of thermal loads in turbomachinery components.

2.3 Computational Fluid Dynamics

Computational Fluid Dynamics (CFD) involves numerically solving the governing equations of fluid motion and, in this case, heat transfer. It is widely utilized to predict complex turbulent flows and thermal interactions in engineering applications [15]. This

section briefly outlines the fundamental CFD approaches and turbulence modeling methods applied in this thesis, including Reynolds-Averaged Navier-Stokes (RANS), Unsteady RANS (URANS), and specific turbulence models utilized for accurately capturing heat transfer phenomena in turbomachinery.

2.3.1 RANS Formulation

The Reynolds-Averaged Navier-Stokes (RANS) equations are a time-averaged form of the Navier-Stokes equations and are commonly used in engineering simulations to model turbulent flows. For compressible flow, the RANS equations consist of the continuity and momentum equations:

$$\frac{\partial \overline{u_i}}{\partial x_i} = 0, \tag{2.5}$$

$$\frac{\partial \overline{u_i}}{\partial t} + \overline{u_j}\frac{\partial \overline{u_i}}{\partial x_j} = -\frac{1}{\rho}\frac{\partial \bar{p}}{\partial x_i} + \nu\frac{\partial^2 \overline{u_i}}{\partial x_j^2} - \frac{\partial \overline{u_i' u_j'}}{\partial x_j} \tag{2.6}$$

Here, $\overline{u_i}$ is the time-averaged velocity, $\bar{p}$ is the mean pressure, ρ is fluid density, ν is the kinematic viscosity, and $\overline{u_i' u_j'}$ represents the Reynolds stress tensor. This tensor introduces additional unknowns which require turbulence modeling to close the system.

In many practical cases, particularly when dealing with relatively low-speed flows (Mach number < 0.3), the assumption of incompressible flow is made to simplify the governing equations. Under this assumption, fluid density is treated as constant, which effectively removes compressibility effects such as density-driven pressure waves from the solution. This approximation reduces computational cost and is typically sufficient for accurately capturing the flow behavior in low-speed regimes.

2.3.1.1 Unsteady RANS (URANS)

In steady-state RANS simulations, the time derivative $\frac{\partial \overline{u_i}}{\partial t}$ is neglected, simplifying the equations and reducing computational cost. However, retaining this term results in the unsteady RANS (URANS) formulation, which captures time-dependent phenomena such as vortex shedding, unsteady separation, and oscillatory boundary layer behavior. URANS is suitable when evaluating cases where transient flow structures and unsteady flow behaviour are important factors.

2.3.2 Turbulence Modeling

Turbulence modeling provides a way to approximate the effects of turbulent fluctuations without directly resolving all turbulent scales. This section outlines the turbulence models relevant to this work.

2.3.2.1 Definition of Various Turbulence Quantities

When working with turbulence models in CFD, turbulence is typically characterized using one of two variable pairs: either the combination of turbulent kinetic energy (k) and

dissipation (either dissipation rate ε or specific dissipation rate ω), or the combination of turbulence intensity (I) and turbulence length scale (L).

Turbulence kinetic energy represents the energy per unit mass associated with the velocity fluctuations in a turbulent flow. It is a measure of the intensity of turbulence and is defined as:

$$k = \frac{1}{2}\overline{u_i' u_i'} \tag{2.7}$$

where u_i' are the fluctuating components of the velocity field. In RANS models, k is a key transported variable that helps characterize the energy in the turbulent eddies.

Turbulence eddy dissipation ε represents the rate at which turbulent kinetic energy is converted into thermal energy due to viscous effects at the smallest scales of turbulence. It is defined as:

$$\varepsilon = \nu \overline{\frac{\partial u_i'}{\partial x_j} \frac{\partial u_i'}{\partial x_j}} \tag{2.8}$$

where ν is the kinematic viscosity and $\frac{\partial u_i'}{\partial x_j}$ are the gradients of the fluctuating velocity components. The k-ε turbulence model uses k and ε as input parameters and is widely used due to its robustness and relatively low computational cost, although it can be less accurate in flows with strong pressure gradients or near-wall effects without additional damping functions.

The specific dissipation rate ω is defined as the eddy dissipation per unit turbulent kinetic energy:

$$\omega = \frac{\varepsilon}{C_\mu k} \tag{2.9}$$

where $C_\mu = 0.09$ is an empirical constant in ANSYS Fluent. Specific dissipation rate has a unit of inverse time (s^{-1}) and characterizes the turbulence time scale. The k-ω turbulence model uses k and ω as its primary variables and is known for its robustness near wall boundaries.

These pairs (k-ε, or k-ω) are directly solved for in two-equation turbulence models such as SST k–ω (see more under section 2.3.2.2) and form the basis of the model's closure of the RANS equations.

Turbulence intensity is a non-dimensional measure of the magnitude of turbulent fluctuations relative to the mean flow velocity. It is often derived from the turbulence kinetic energy and can, assuming isotropic conditions, be formulated accordingly:

$$u' = \sqrt{\frac{2}{3}k}, \quad U = \sqrt{U_i^2 + U_j^2}, \tag{2.10}$$

$$I = \frac{u'}{U} = \sqrt{\frac{2k}{3(U_i^2 + U_j^2)}} \tag{2.11}$$

Turbulence length scale characterizes the size of the dominant eddies in the turbulent flow field. Unlike turbulence intensity, it is not directly derived from k and ω without additional assumptions. It typically requires a combination of empirical correlations and model-dependent definitions. ANSYS Fluent provides the following estimate:

$$L = v_t \cdot \tau, \tag{2.12}$$

$$v_t = \max(v_m, v_k), \quad \tau = \max(\tau_m, \tau_k), \tag{2.13}$$

$$v_m = \sqrt{k}, \quad v_k = \left(\frac{\varepsilon\mu}{\rho}\right)^{1/4}, \tag{2.14}$$

$$\tau_m = \frac{k}{\varepsilon}, \quad \tau_k = \sqrt{\frac{\mu}{\rho\varepsilon}} \tag{2.15}$$

Meanwhile, ANSYS CFX uses a simplified definition:

$$L = \frac{k^{3/2}}{\varepsilon} \tag{2.16}$$

2.3.2.2 SST k–ω Model

The Shear Stress Transport (SST) k–ω model is a widely used two-equation eddy-viscosity turbulence model. It solves two transport equations; one for the turbulent kinetic energy k and one for the specific dissipation rate ω. These two variables represent the intensity and the scale of turbulence, respectively.

The transport equation for turbulent kinetic energy k is:

$$\frac{\partial k}{\partial t} + \overline{u}_j \frac{\partial k}{\partial x_j} = P_k - \beta^* k\omega + \frac{\partial}{\partial x_j}\left[(\nu + \sigma_k \nu_t)\frac{\partial k}{\partial x_j}\right] \tag{2.17}$$

The transport equation for specific dissipation rate ω is:

$$\frac{\partial \omega}{\partial t} + \overline{u}_j \frac{\partial \omega}{\partial x_j} = \alpha \frac{\omega}{k} P_k - \beta\omega^2 + \frac{\partial}{\partial x_j}\left[(\nu + \sigma_\omega \nu_t)\frac{\partial \omega}{\partial x_j}\right] \tag{2.18}$$

where:

- P_k is the production of turbulent kinetic energy,
- ν_t is the eddy viscosity,
- α, β, β^*, σ_k, and σ_ω are empirical constants.

This turbulence model combines features from both the $k-\varepsilon$ and standard $k-\omega$ models ($k-\varepsilon$ is not used in this thesis and is therefore not explained further). In near-wall regions, it employs the $k-\omega$ formulation, which accurately resolves the turbulent boundary layer behavior without requiring wall functions. Away from the walls, the model switches to a $k-\varepsilon$ formulation to leverage better free-stream turbulence prediction capabilities. This blending depends on the shear stress close to the wall and ensures robust and accurate modeling of flows characterized by strong adverse pressure gradients, separation, and near-wall turbulence phenomena. However, it assumes fully turbulent conditions and thus requires further augmentation to resolve transitional phenomena.

2.3.2.3 γ–Re_θ Transition Model

To capture transitional flow behavior, the γ–Re_θ model is employed. This model extends the SST $k-\omega$ model by explicitly modeling laminar-to-turbulent boundary layer transition. This is thus called a transition model and introduces two additional variables on top of the turbulence kinetic energy and specific dissipation rate:

- γ – intermittency, a scalar between 0 and 1 describing the fraction of time the flow is turbulent. A value of 1 means the flow if fully turbulent while a value of 0 represents fully laminar flow behaviour.
- Re_θ – the local transition onset momentum thickness Reynolds number given by

$$\mathrm{Re}_\theta = \frac{\rho V \theta}{\nu}, \tag{2.19}$$

  where θ is the momentum thickness which is used to quantify the thickness of the boundary layer in fluid flows. The momentum thickness can be described using the following correlation:

$$\theta = \int_0^\infty \frac{\rho U}{\rho_\infty U_\infty}\left(1 - \frac{U}{U_\infty}\right) dy \tag{2.20}$$

The governing transport equations for intermittency and momentum thickness are:

$$\frac{\partial \gamma}{\partial t} + \overline{u}_j \frac{\partial \gamma}{\partial x_j} = P_\gamma - E_\gamma + \frac{\partial}{\partial x_j}\left[(\nu + \sigma_\gamma \nu_t)\frac{\partial \gamma}{\partial x_j}\right] \tag{2.21}$$

$$\frac{\partial Re_\theta}{\partial t} + \overline{u}_j \frac{\partial Re_\theta}{\partial x_j} = P_{Re_\theta} + \frac{\partial}{\partial x_j}\left[(\nu + \sigma_{Re_\theta} \nu_t)\frac{\partial Re_\theta}{\partial x_j}\right] \tag{2.22}$$

The intermittency equation tracks the development of turbulence intermittency along surfaces, while the Re_θ equation predicts the point of transition onset based on local flow conditions and free-stream turbulence. By solving these equations simultaneously with the SST $k-\omega$ model, the γ-Re_θ model provides a robust and reliable framework for accurately predicting transitional flows.

The γ-Re_θ model is particularly crucial in certain turbomachinery applications where accurate prediction of the heat transfer coefficient (HTC) at the leading edge of vanes and blades is highly sensitive to the transition location and behavior.

2.3.3 Flow Transition

In fluid mechanics, boundary layer flow can exist in laminar, transitional, or fully turbulent regimes. While laminar flow is characterized by smooth, orderly layers with minimal mixing, and turbulent flow by chaotic, vortical structures with significant momentum

exchange, transitional flow lies between the two. It is a highly sensitive regime where even small disturbances in the velocity or pressure field can grow and trigger turbulence.

Flow transition refers to the process by which initially laminar boundary layers become unstable and develop into turbulent flow. This process is governed by several factors including local Reynolds number, surface roughness, free-stream turbulence intensity, pressure gradients, and upstream disturbances such as wakes. Figure 2.2 shows a simple example case where a flat plate is subject to a flow from right to left. When the flow hits the flat plate, the boundary layer is very thin at first which leads to a high HTC. The boundary layer gradually increases in thickness, leading to a decrease in HTC. The flow then starts to transition, exhibiting turbulent behaviour and mixing in the boundary layer which increases the HTC. The flow transitions to fully turbulent with a local HTC peak, which then decreases slightly as the boundary layer increases in thickness and the turbulent structures stabilize.

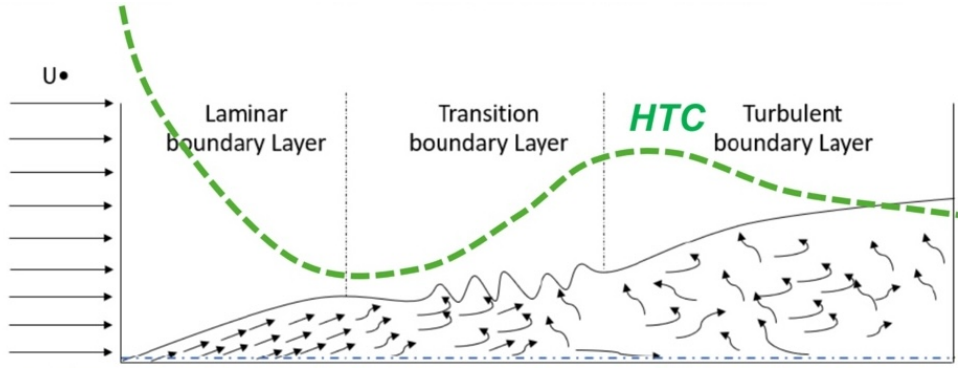

Figure 2.2: Depiction of flow transition from laminar to turbulent and how the HTC is affected.

2.3.3.1 Importance in Turbomachinery

In turbomachinery, especially in the LPT and TRS, the operating Reynolds numbers are often in the transitional range (typically 10^4–10^6), making transition phenomena highly relevant. Unlike external aerodynamic surfaces, these components are subjected to significant free-stream turbulence, wake impingement from upstream blades, and strong adverse pressure gradients. These factors contribute to various transition mechanisms, including:

- **Bypass transition:** triggered directly by free-stream turbulence or upstream wake structures, bypassing natural linear instability routes.
- **Separation-induced transition:** occurs when a laminar boundary layer separates, transitions to turbulence in the shear layer, and then reattaches.
- **Wake-induced transition:** caused by periodic fluctuations from upstream blades impacting the boundary layer stability.

2.3.3.2 Implications for CFD and Design

Accurately predicting transition is critical for thermal analysis and fatigue prediction. Using fully turbulent models like SST k–ω without transition modeling can overpredict HTC in the laminar region (front-most section of the vane) by 30–50%, leading to exaggerated design margins. This is why dedicated transition models, such as the γ–Re_θ model, are essential in resolving laminar-turbulent behavior and capturing the resulting HTC distributions. In short, neglecting transition can lead to:

- Low accuracy on evaluating point of transition along blades/vanes, or even complete exclusion of transitional behaviour
- Misplacement of peak HTC locations
- Overestimation of leading edge thermal loads
- Incorrect boundary layer development, influencing downstream wake behavior

2.3.4 Characteristic Numbers

The following non-dimensional numbers are fundamental tools to characterize different flow regimes and transport phenomena.

- Firstly, the **Reynolds number** is given as

$$Re = \frac{\rho u L}{\mu} \tag{2.23}$$

  where ρ is the density, u is the flow velocity, L is the characteristic length, and μ is the dynamic viscosity. The Reynolds number specifies whether a flow is laminar or turbulent, where general ranges of $Re_{lam} < 50\,000$ and $Re_{turb} > 250\,000$ are valid for turbomachinery flows. $50\,000 < Re < 250\,000$ is the domain where the flow transitions from laminar to turbulent.

- The **Prandtl number** describes how the temperature propagates through fluids in relation to the flow velocity. In other words, it compares the momentum diffusion with thermal diffusion:

$$Pr = \frac{\nu}{\alpha} = \frac{c_p \mu}{k} \tag{2.24}$$

  where ν is the viscosity, α is the thermal diffusivity, c_p is the specific heat capacity, μ is the dynamic viscosity, and k is the thermal conductivity.

- The **Nusselt number** determines the relation between convective heat transfer and conductive heat transfer across a boundary layer:

$$Nu = \frac{hL}{k} \tag{2.25}$$

  where h is the convective heat transfer coefficient, L is the characteristic length, and k is the thermal conductivity.

Following this, the **Frössling number** combines the Reynolds and Nusselt numbers accordingly:

$$Fr = Nu \cdot Re^{-0.5} \tag{2.26}$$

This relation is especially relevant for cases where the convective heat transfer is influenced by both the flow regime and the thermal boundary layer. A high Frössling value indicates that the heat transfer is dominated by convective heat transfer, while a low Frössling value points to a more turbulent flow.

- **Eddy Viscosity Ratio** compares the turbulent (eddy) viscosity to the molecular (laminar) viscosity. It reflects the relative importance of turbulence-induced momentum transport compared to molecular diffusion in a flow. In turbulence models like k-ω, the eddy viscosity is modeled to account for the additional momentum transfer caused by turbulent eddies. The eddy viscosity ratio is defined as

$$\frac{\nu_t}{\nu} \tag{2.27}$$

where ν_t is the eddy viscosity and ν is the kinematic viscosity. A higher eddy viscosity ratio indicates dominant turbulent mixing, while a value near 1 or lower suggests laminar or low-turbulence conditions.

- The $\boldsymbol{y^+}$**-number** is a non-dimensional parameter used to assess whether the computational mesh near a wall is fine enough to accurately resolve the boundary layer in CFD simulations. It is defined as

$$y^+ = \frac{yu_\tau}{\nu}, \tag{2.28}$$

where y is the distance to the wall from the first cell center, ν is the kinematic viscosity of the fluid, and u_τ is the friction velocity defined as

$$u_\tau = \sqrt{\frac{\tau_w}{\rho}} \tag{2.29}$$

where τ_w is the wall shear stress and ρ is the density of the fluid. y^+ is essential to ensure that the mesh resolution is fine enough in the viscous sub-layer where the temperature and velocity gradients are the steepest. This is of utmost importance since a resolved boundary layer is necessary for predictions of wall heat transfer (amongst many more). When using some form of the $k-\omega$ turbulence model (like in this thesis work) and when modelling heat transfer, a y^+ value of less than 1 is generally necessary to resolve the viscous sublayer and thermal boundary layer.

- Lastly, the **CFL number** (Courant-Friedrichs-Lewy-number), often referred to as the Courant number, is used in CFD to ensure numerical stability in simulations. It is expressed as

$$CFL = \frac{u\Delta t}{\Delta x} \tag{2.30}$$

where u is the flow velocity, Δt is the time step size, and Δx is the distance between neighbouring grid points of the relevant mesh cells. Simply put, the CFL number represents the ratio of the distance a fluid flows in one time step to the cell length. Generally speaking, the CFL number should not exceed 1 for explicit numerical schemes while a higher CFL number (CFL $<$ 5-10) can be accepted for implicit methods, depending on the specific case.

3
Methodology

Both steady-state and transient 2D models were developed throughout this project. While the primary objective was to investigate unsteady effects using the transient approach, the steady-state model served as a baseline reference to assess the impact of unsteadiness. The procedures and case-specific approaches used when developing these models are described in detail, including simplifications and creation of different geometries, meshing strategies, imposing of boundary conditions, and solver settings.

Before proper simulation models and mesh studies were done using actual geometries, boundary conditions and performing, simpler cases using cylinders instead of blades/-vanes were developed. This preliminary step allowed for gaining familiarity and proper understanding of the software tools and also provided essential insights into the relevant thermodynamic and aerodynamic phenomena. It ensured a clear and effective progression toward the more complex models described in detail in the following sections.

3.1 Software Used

The following software were used throughout this work:

- **Geometry:** ANSYS SpaceClaim and DesignModeler. Already developed 3D geometries were manipulated and converted to 2D.
- **Mesh:** ANSYS Meshing through Workbench.
- **Solver:** ANSYS Fluent.
- **Posting:** ANSYS Fluent and CFD-Post. Fluent was used for efficient time-averaging, while CFD-Post was used for temporal/instantaneous result analysis.

3.2 Reference Models Used

Three main reference models and data sources were used extensively throughout this work:

- The 1.5-stage steady-state CFD simulation model developed by GKN
- The Chalmers Test Rig
- GKN internal data

These models are used to extract geometries as well as relevant boundary conditions, depending on the simulation model. They will therefore be clearly differentiated to prevent

potential ambiguities.

The 1.5-stage CFD model refers to a three-dimensional steady-state model developed by GKN. Both the geometry and simulation setup was developed in-house. It consists of one stator, one rotor and one OGV according to figure 3.1. While it does not capture transient flow phenomena, it provides a dataset from which key boundary conditions can be extracted.

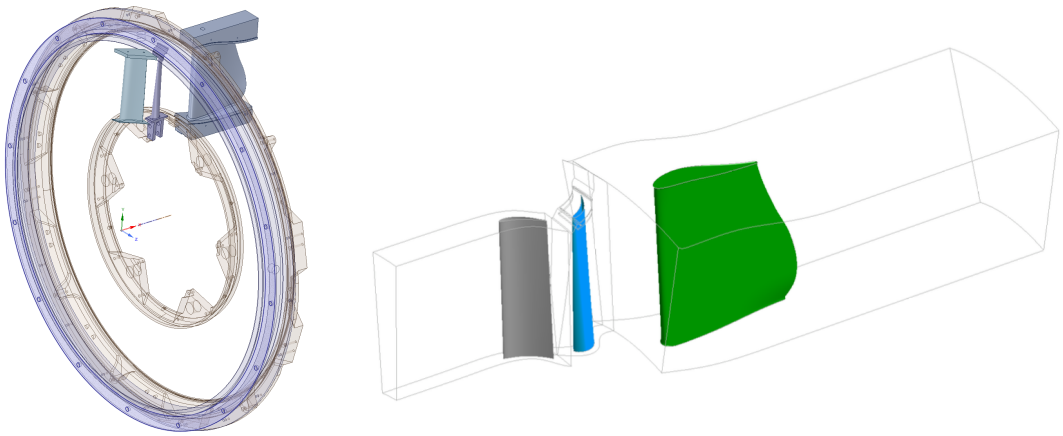

Figure 3.1: CAD-model of the 1.5-stage configuration (left) and the CFD steady-state model developed using the same geometry (right).

The Chalmers Test Rig (CTR), as explained previously, is an experimental facility used to perform thermal measurements on the OGV. The geometry is taken in full from the 1.5-stage model at GKN. These experimental results are used as a benchmark for validating numerical results and assessing simulation model accuracy. The CTR provides HTC measurements as well as thermal boundary conditions used in the CFD models.

Lastly, GKN internal data regarding turbulence quantities at the OGV inlet is also available. This data comes from previous work and experience from other similar projects.

These three sources were used to extract geometries as well as boundary conditions. This is discussed in more detail in upcoming sections.

3.3 Geometry

The transient model included both the rotors and OGVs, allowing it to capture the unsteady wake effects generated by the upstream rotor blades. In contrast, the steady-state model consisted solely of the OGV domain and therefore did not account for any upstream unsteady influences. This distinction is crucial, as the inclusion of the rotor domain in the transient model enables a more realistic simulation of the flow physics impacting the OGV.

3.3.1 Transient Model

Using the geometry from GKN, a planar cut at the OGV leading edge midspan was made according to figure 3.2.

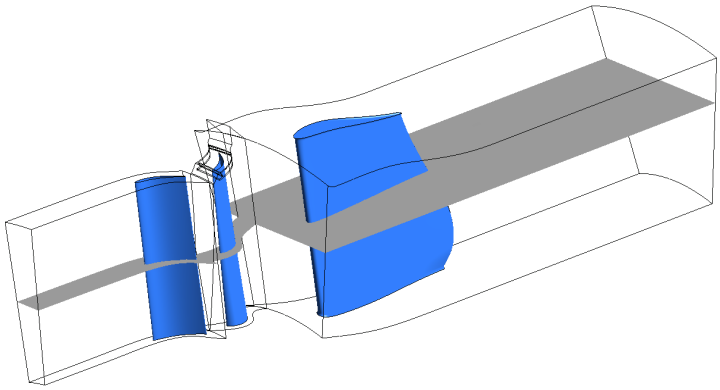

Figure 3.2: 3D model with planar cut at OGV leading edge midspan

The number of rotor blades and OGVs is 72 and 12, respectively. This means that the smallest periodically symmetric sector of the model is $\frac{360}{12} = 30$ degrees. Consequently, the number of rotors and OGVs in this sector is 6 and 1, respectively. A 2D representation of this 30 degree sector was then developed according to figure 3.3.

Figure 3.3: 2D geometry including rotor and OGV domain, used for transient simulations.

The 2D transient model is also cut into two separate domains - referred to as the rotor domain and OGV domain. This has to be done in order to allow for the sliding mesh which is discussed in more detail under section 3.5.

3.3.2 Steady State Model

While the transient simulation model contains both the rotor and OGV domain, the steady model will only include the OGV domain as shown in figure 3.4. This was done to be able to compare two different cases: one transient model including unsteady upstream rotor effects, and one steady model without upstream effects.

Figure 3.4: 2D geometry only including the OGV domain, used for steady simulations.

3.4 Mesh Generation and Convergence Study

Mesh resolution is a critical aspect of this study as it is of utmost importance that the model accurately resolves unsteady turbulence structures and heat transfer behavior, both in the bulk flow and near the solid surfaces. More specifically, the mesh has to be fine enough to capture and maintain turbulence structures generated from the upstream rotor blades until they reach the OGV, and not allow them to dissipate early due to numerical diffusion. A sufficiently fine mesh is needed at the rotor and OGV surfaces in order to resolve the aerodynamic and thermal behaviour in the boundary layer region. While over-refined meshes may be acceptable in steady-state simulations, where computational cost scales slower and time-resolved flow phenomena are not of concern, the same approach becomes unsustainable for transient simulations. Excessive refinement in such cases leads to significantly increased computation times, disk usage, and time step constraints due to the CFL condition.

The primary requirement in this work was thus to construct a mesh that was fine enough to resolve the HTC distribution along the OGV surface while minimizing the number of cells in the model. To achieve this, three mesh configurations - coarse, medium, and fine - were created and evaluated through a mesh independence study. The convergence was assessed by evaluating OGV leading edge HTC levels, residuals, as well as contours of velocity and turbulence quantities. The results from the mesh study can be found under section 4.2.

An example mesh exhibiting the general characteristics of the three mesh sizes can be seen in figure 3.5. It depicts the mesh of the full model as well as a close-up of the rotor blade trailing edge.

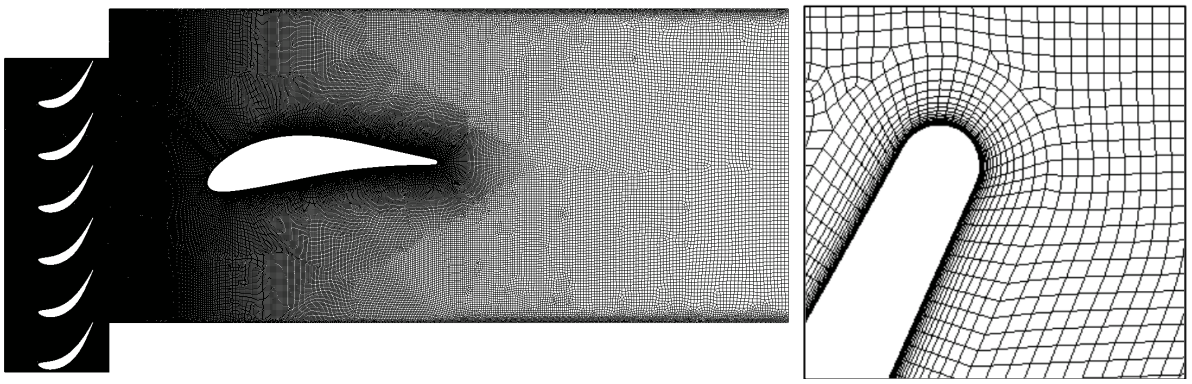

Figure 3.5: General representation of the mesh layout used - full mesh (left) and rotor blade trailing edge close-up showing inflation layers(right).

The mesh comprises two domains: the rotor and the OGV. The mesh in the rotor domain was kept at a uniform resolution to resolve the incoming flow field, whereas the OGV domain features a gradual increase in cell size in the stream-wise direction toward the outlet. This coarsening reduces overall cell count while ensuring that the leading edge and aft of the OGV retain sufficient fidelity. It is this region between the rotor trailing edge and the OGV leading edge that is of importance since this is where the wakes are generated and then travels downstream to the OGV surface. Great care was thus taken to ensure that this coarsening did not lead to early dissipation of important flow structures before they reached the OGV.

Boundary layer resolution was handled using inflation layers at all rotor blades and the OGV. A total of 24 layers with a growth rate of 1.25 were applied, and the mesh was refined to ensure $y^+ < 1$ at all locations. This is essential for the SST-transition turbulence model, particularly when resolving heat transfer near walls. While a y^+ of 0.1 or lower is sometimes necessary for transition models, this was not the case in this study.

Although the rotor-OGV interface (that is, the two edges in contact with each-other) mesh is geometrically conformal, ANSYS Fluent handles it as a non-conformal interface due to the configuration of its sliding mesh functionality. This has no detrimental effect on solution accuracy but is worth noting for reproducibility. In contrast, the top and bottom domain boundaries are fully conformal, facilitating efficient use of periodic boundary conditions which further reduces computational cost.

General mesh quality was verified using internal GKN guidelines. While specific thresholds cannot be disclosed, quality metrics such as skewness, orthogonality, and aspect ratio fell within approved ranges.

3.5 Setting Up the Sliding Mesh

Since the simulations are done in 2D, the rotation of the rotor blades must be replaced by a translational approximation. While this might not exactly capture the rotating characteristics of the turbine stage, it should provide a good estimate of the flow behaviour.

The geometry is split into two different domains - the rotor domain and OGV domain. The OGV domain will remain static, while the rotor domain moves vertically in a periodic manner. Referring to the simplified geometry in figure 3.6 (only used for demonstration purposes) where the left and right domains represent the rotor and OGV domains respectively, the motion will be as follows:

1. The two domains start in a completely connected manner.
2. The rotor domain starts moving downwards.
3. This motion continues until the top edge of the rotor domain reaches the bottom edge of the OGV domain.
4. The position of the rotor domain resets to position 1. This motion is repeated continously.

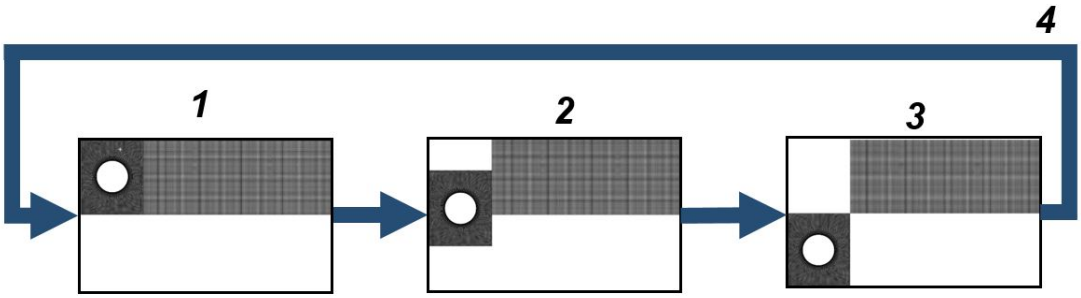

Figure 3.6: Depiction of sliding mesh functionality using arbitrary geometry.

Using the equation for angular velocity, the translational velocity can be calculated accordingly:

$$v = \omega r, \tag{3.1}$$

where v is the translational velocity, ω is the angular velocity, and r is the radius to the mid-span of the turbine stage. Using the test rig dimensions and operating conditions the velocity of the sliding mesh can be computed:

$$\omega \approx 87\text{s}^{-1}, r_{mid} \approx 0.44\text{m} \Rightarrow v \approx 38.3\text{m/s}. \tag{3.2}$$

To accomplish the behaviour of a sliding mesh in ANSYS Fluent, a mesh interface of type "periodic repeats" is implemented. Referring to figure 3.7, this method allows for continuos periodic motion as described above. Furthermore, it also enables certain flow/domain connections. That is, while the rotor domain is moving, some edges (also called "zones") will be overlapping between the two domains while some zones will be non-overlapping. The overlapping zones are directly mapped such that what exits the rotor domain enters the OGV domain and vice versa(see orange arrow). Conversely, the non-overlapping zones are linked to each other in a similar way (see red arrows). This in conjunction with translational periodic boundary conditions on the top and bottom of the two domains give the desired functionality (discussed further under section 3.6.1.3).

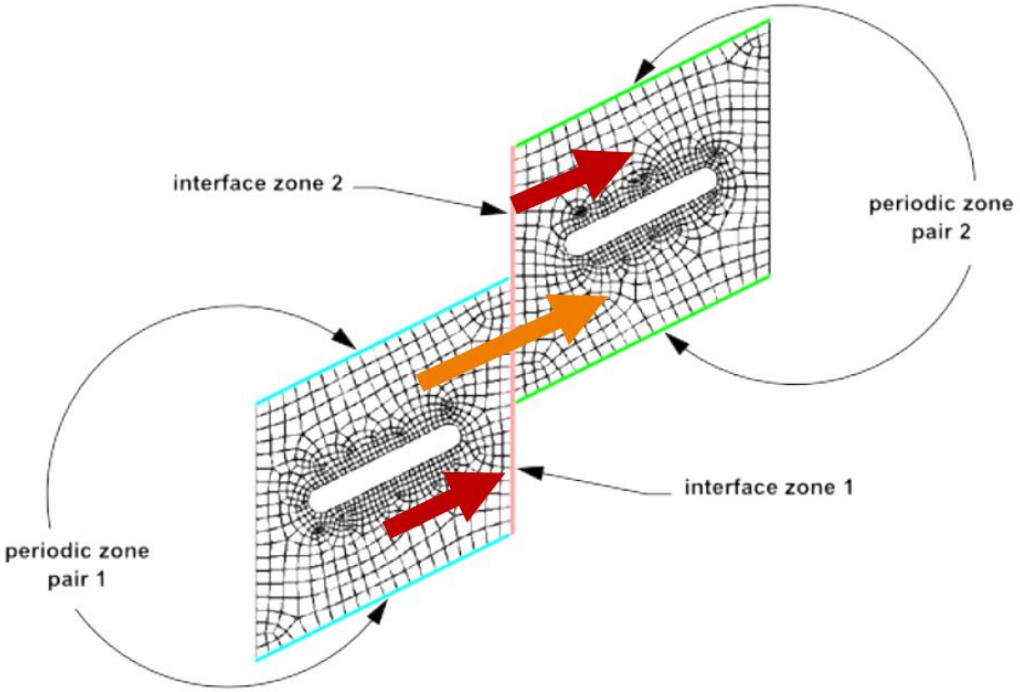

Figure 3.7: Visualisation of Fluent's mesh interface of type "periodic repeats".

Appendix A.1 includes a short guide as to how to properly set up the sliding mesh along with other useful information regarding this setting.

3.6 Boundary Conditions

The boundary conditions used vary depending on the simulation model (steady or transient), but they all stem from the 1.5-stage model, CTR, or GKN internal data (previously established under section 3.2. In the following sections, these boundary conditions will be stated and explained for the transient and steady-state models.

The names of the boundaries and their corresponding location is shown in figure 3.8.

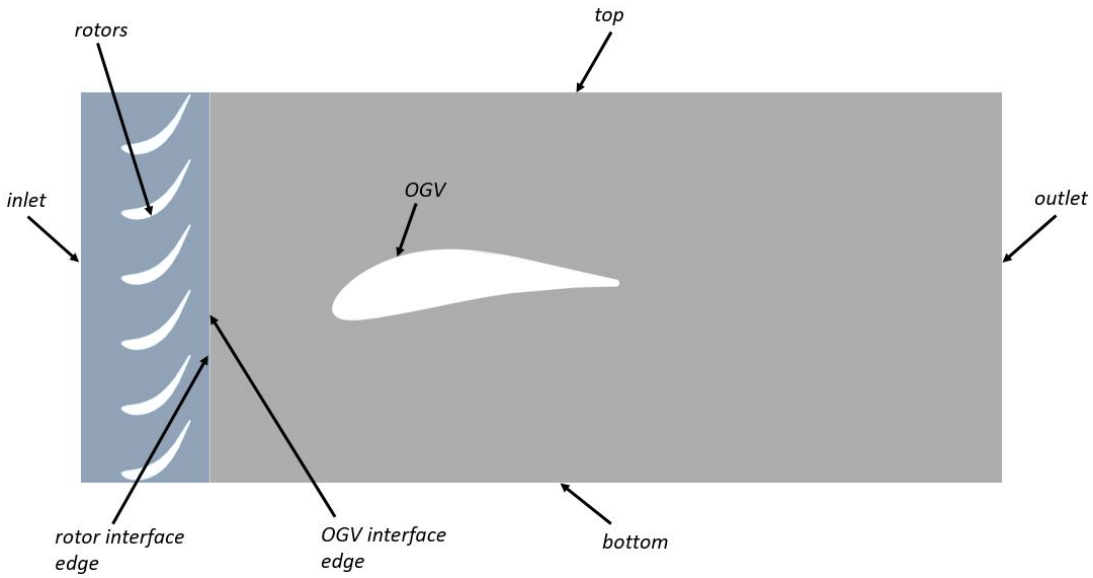

Figure 3.8: Naming of each boundary.

3.6.1 Transient Simulations

Table 3.1 shows the boundary conditions for the transient model.

Table 3.1: Full list of boundary conditions used for the transient model.

	Rotor inlet		Outlet		"Bottom+Top"		Turbine and OGV domain interface edges		Rotor blades		OGV	
BC type	Pressure inlet		Pressure outlet		Periodic		Interface		Wall, no slip		Wall, no slip	
Settings	Total Pressure	103200 Pa	Static Pressure	101325 Pa	Type	Translational	Type	Periodic Repeats	Heat flux	0 (adiabatic)	Temperature	292.15 K
	Direction	(x, y) = (1, -1.5)	Turb. intensity	1%								
	Temperature	302.15 K	Turb. length scale	1e-5 m								
	Turb. kinetic energy	1.547 J/kg										
	Turb. dissipation rate	5195 s^-1										
BC Source	Velocity and turbulence: 1.5-stage model Temperature: CTR		Turbulence: GKN internal data Pressure: CTR								CTR	
Notes	Pressure is set to match the velocity magnitude at the rotor inlet in the 1.5-stage model, equal to 43 m/s								Prevents rotor blade heat flux from affecting results		10 degrees cooler than the air	

3.6.1.1 Inlet and Outlet - Pressure

The pressure at the outlet was set to ambient conditions (1atm) like in the CTR. A higher pressure was then set along the inlet to induce a flow from inlet to outlet. The pressure difference was adjusted to get a velocity at the rotor inlet (magnitude and direction) that matched with the 1.5-stage model. The turbulence quantities (in the form of turbulence kinetic energy and specific dissipation rate) were also extracted from the 1.5-stage model since this is the only available data for turbulence at the rotor inlet. The temperature of the inlet air flow was taken from the CTR.

While a velocity inlet boundary could be used, this led to backflow issues downstream of

the OGV. The reason for this can be explained using the definitions ANSYS Fluent uses for its pressure boundaries.
Firstly, gauge pressure in ANSYS Fluent is defined as

$$p_{gauge} = p_{abs} - p_{oper} = p_{abs} - 0 = p_{abs} \tag{3.3}$$

where the operating pressure is set to zero according to ANSYS Fluent's user manual for models with Mach numbers lower than 0.3.
Setting the gauge pressure to zero gives the following:

$$p_{gauge} = 0 \Rightarrow p_{abs} = 0 \tag{3.4}$$

Pressure inlets in ANSYS Fluent is defined using total pressures, while pressure outlet is defined using static pressures. The pressure drop Δp from the inlet (1) to the outlet (2) can be written as

$$p_{01} = p_1 + \frac{1}{2}\rho v^2 \tag{3.5}$$

$$\Delta p = p_1 - p_2 \tag{3.6}$$

Since the pressure outlet boundary condition is defined as static pressure, this means the pressure at the outlet will remain constant:

$$p_2 = \text{constant} \Rightarrow \Delta p = p_{01} - \frac{1}{2}\rho v^2 \tag{3.7}$$

$$\frac{1}{2}\rho v^2 > p_{01} \Rightarrow \Delta p < 0 \Rightarrow p_2 > p_1 \tag{3.8}$$

which shows that defining an inlet velocity together with a pressure outlet can easily lead to backflow issues. The only available data for inlet velocities and outlet pressure is from the 1.5-stage model which is a steady 3D model. Thus, it is not possible to use the available 3D data in these 2D simulations, which is why a pressure inlet was used instead.

3.6.1.2 Rotor Blades and OGV - Wall

The rotor blades and OGV are set to walls with no-slip condition. The rotor blades are set to adiabatic as the thermal conditions here are unknown. The OGV is set to a constant temperature of 10 degrees cooler than the inlet flow, as to induce a heat flux allowing for HTC evaluation.

3.6.1.3 Top and Bottom - Periodic

In order to account for the fact that only a 30 degree sector is included in the simulation, periodic boundaries are used for the top and bottom. Using this boundary condition in conjunction with the sliding mesh interface allows for the desired cascade-like system. The periodicity type is translational (as opposed to rotational) since a 2D planar model is used. It is worth noting that while meshes with non-conformal cells along the top and bottom will work, a conformal mesh is preferred since it decreases computation time.

3.6.1.4 Interface Edges - Sliding Mesh

The behaviour of this boundary condition has already been explained under section 3.5 (*Setting Up the Sliding Mesh*). Once again, while the general name for this type of boundary is called sliding mesh, ANSYS Fluent refers to it as a mesh interface boundary of type "periodic repeats". Using a non-conformal or conformal mesh does not make a difference in computational efficiency for this type of boundary since Fluent always interprets and solves it as non-conformal.

3.6.2 Steady State Simulations

The steady model will be run using two different sets of turbulence boundary conditions at the OGV inlet.

The first setup is seen in table 3.2, where the turbulence quantities are taken from GKN internal data. This data has been developed such that the simulation exhibits natural and realistic behaviour regarding turbulence kinetic energy and eddy viscosity ratios to prevent so called "honey-spots" where the eddy viscosity reaches unreasonable levels. This is also the turbulence data used in previous 3D simulations by Murali in 2023.

Table 3.2: Full list of boundary conditions used for the steady model with turbulence from GKN internal data.

	OGV inlet		**Outlet**		**"Bottom+Top"**		**OGV**	
BC type	Velocity inlet		Pressure outlet		Periodic		Wall, no slip	
Settings	velocity mag	25 m/s	Static Pressure	101325 Pa	Type	Translational	Temperature	292.15 K
	direction	(x, y) = (3.2; 1)	Direction	Previous cell				
	Temperature	302.15 K	Turb. intensity	1%				
	Turb. intensity	5%	Turb. length Scale	1e-5 m				
	Turb. length Scale	0.0012m						
BC Source	Velocity: 1.5-stage model Turbulence: GKN internal data		Turbulence: GKN internal data Pressure: CTR				CTR	
Notes			1atm (like ambient conditions in CTR)				10 degrees cooler than the air	

The second setup contains turbulence quantities from the transient model, extracted at the OGV inlet as shown in table 3.3. The turbulence is imposed in the steady model in time-averaged quantities. This model allows for direct comparison of the steady and transient models without having to take into consideration the potential differences in turbulence upstream of the OGV.

Table 3.3: Full list of boundary conditions used for the steady model with turbulence quantities extracted from the transient model.

	OGV inlet		Outlet		"Bottom+Top"		OGV	
BC type	Velocity inlet		Pressure outlet		Periodic		Wall, no slip	
Settings	velocity mag	25 m/s	Static Pressure	101325 Pa	Type	Translational	Temperature	292.15 K
	direction	(x, y) = (3.2; 1)	Direction	Previous cell				
	Temperature	302.15 K	Turb. intensity	1%				
	Turb. kinetic energy	2.2 J/kg	Turb. length Scale	1e-5 m				
	Turb. dissipation rate	18210 s^-1						
BC Source	Velocity: 1.5-stage model Turbulence: transient model		Turbulence: GKN internal data Pressure: CTR				CTR	
Notes	Turbulence from transient model used to evaluate differences between turbulence levels		1atm (like ambient conditions in CTR)				10 degrees cooler than the air	

3.7 Solver Setup and Flow Development

Key settings and setup-parameters used in the simulations are presented below:

- A pressure-based solver was used due to the low velocities. Evidently this would not be the case if using real operating conditions, but considering that the CTR is operated at ambient conditions made this an obvious choice.
- The transition-SST turbulence model is used, based on earlier findings by Murali (2023).
- The SIMPLE-scheme was used to run the transient simulations. This allowed for similar predictions of the HTC compared to the SIMPLEC, PISO and Coupled schemes, while decreasing total run time by up to 50%. The steady model was run using the Coupled algorithm since it provided the fastest and most stable convergence.
- A time step size of 1e-5s was used along with 10 inner iterations (given the results from the mesh study). CFL number sensitivity was evaluated to confirm that a smaller time step was not necessary for the given mesh.
- The transient model was run for 40 000 time steps, or 0.4s, before exporting of data was initiated. Before any post-processing could be performed, it was first necessary to allow the flow field to reach a fully developed and periodically converged state. This was evaluated by monitoring the temporal fluctuations of the HTC at the OGV stagnation point. Once this had reached a steady periodic behaviour, data export was initiated.

3.8 Simulation Scripts and Case Configurations

To efficiently manage the large number of simulation cases and gradual changes in simulation setup required for this thesis, a set of custom simulation scripts were developed using ANSYS TUI language to automate the solver execution of both transient and steady-

state cases. This scripting approach significantly reduced the risk for human error while streamlining the workflow, making it easy to make quick adjustments in between runs. The scripts handled tasks such as:

- Importing case and mesh files
- Defining all relevant boundary conditions
- Initializing and running the simulation in batch mode
- Extracting surface- and volume-averaged data
- Exporting data, both instantaneous and time-averaged
- Automating convergence checks and file naming for result archiving

An example of a simulation script for one of the transient simulations can be found in appendix A.2.

3.8.1 Data Export and Post-Processing

In transient simulations, large volumes of data are generated over time. To manage this effectively, careful consideration was given to both when data should be exported and what quantities should be monitored or extracted. The primary objective was to obtain high-resolution and representative datasets of key flow and thermal quantities - such as the HTC, velocity and pressure fields, and turbulence parameters - while minimizing unnecessary disk usage and computational burden.

To minimize disk usage and avoid unnecessary transient noise when time-averaging the data, the following export strategy was adopted:

- Initial transient results during flow development were discarded, and only data from the periodically developed time frame of the simulation was saved.
- Data was exported every 20 time steps, used to evaluate temporal fluctuations in CFD-Post.
- Time-averaged flow quantities were also computed using Fluent's built-in averaging tools.

3.9 Final Comparisons and Conclusions

Post-processed data from different simulation configurations - transient and steady state - were compiled into a consistent format to allow for direct and clear comparisons and validation. Key metrics used for evaluation included:

- HTC profile distribution and magnitude (both instantaneous and time-averaged for transient case)
- Stagnation point HTC variations through time (for transient case)
- Velocity magnitude
- Turbulence quantities

The following datasets form the basis for the comparative analysis:

- Previous 3D model - This model was cut at the midspan to be able to evaluate it against the newly developed 2D models.
- 2D steady state models – using turbulence boundary conditions from (i) GKN internal data, and (ii) the time-averaged transient simulation
- 2D transient model
- Experimental data from the Chalmers test rig

4
Results

First, the quality of the geometry is discussed. This is followed by the mesh convergence study and a depiction of the chosen mesh resolution.

The simulation results are then presented, starting with a comparison between the 3D steady and 2D steady model. The results from the transient model is then presented, and is compared to the 2D steady models and the experimental data. Finally, all four cases (3D steady, 2D steady, 2D transient, and experimental data) are compared.

4.1 CAD Geometry Fidelity

Upon close inspection of the imported parasolid geometry from GKN, it became clear that the shape definition lacks sufficient resolution for fine mesh simulations. Figure 4.1 shows this clearly: when using a fine mesh, the OGV profile exhibits "stair-stepping" or jagged behavior at the leading edge due to the jagged CAD surface.

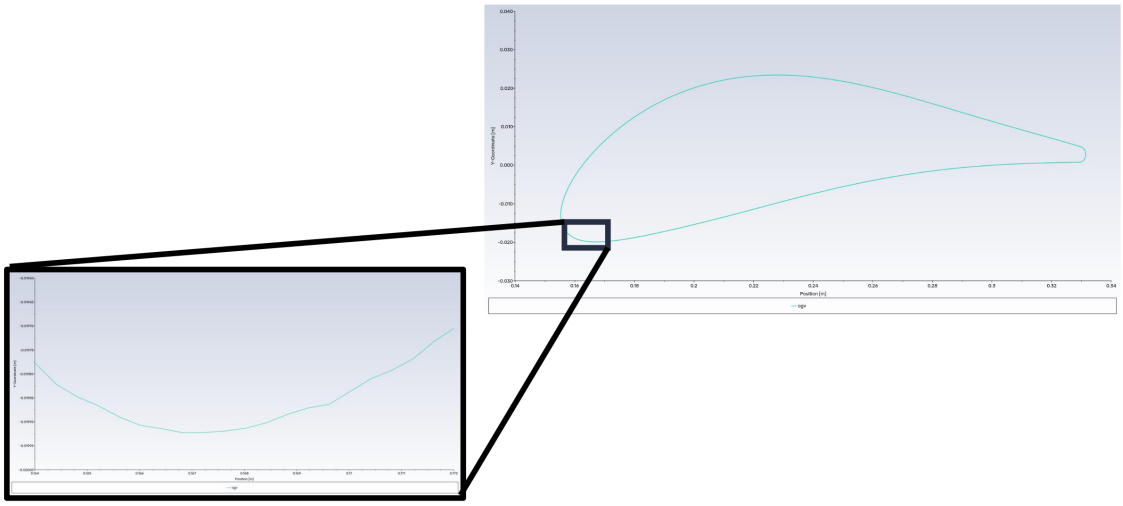

Figure 4.1: Depiction of low resolution OGV profile, with close-up of leading edge

This effect causes local HTC peaks to become erratic, especially in high-gradient regions near the stagnation point and in areas of rapid transition (shown in upcoming sections). However, using a coarser mesh smooths out the surface and prevents this issue — albeit at the expense of possibly capturing finer flow structures. This further confirms that the jagged HTC predictions are due to the geometry's lower quality. It is however believed

that the general HTC trend and magnitude should be preserved, and that while the contour "noise" was visible, the overall thermal predictions should remain robust.

4.2 Mesh Requirements

Before presenting the results of the mesh study, it is important to clarify a key point. At the time when the convergence study was performed, incorrect inlet boundary conditions were used due to an error when extracting these from the 1.5-stage CFD model. As a result, the simulated flow conditions were closer to off-design operation, which led to more pronounced vortex shedding, flow separation at the rotor leading edge, and increased turbulence levels. Once this issue was identified, there was not enough time to repeat the mesh convergence study with the corrected boundary conditions. Therefore, the decision was made to proceed with the existing results. This decision and its implications are further discussed in section 5.2.

Three different mesh sizes were evaluated: coarse (cell edge length 4e-4m), medium (cell edge length 2e-4m), and fine (cell edge length 1e-4m). The turbulence kinetic energy for each mesh is shown in figure 4.2.

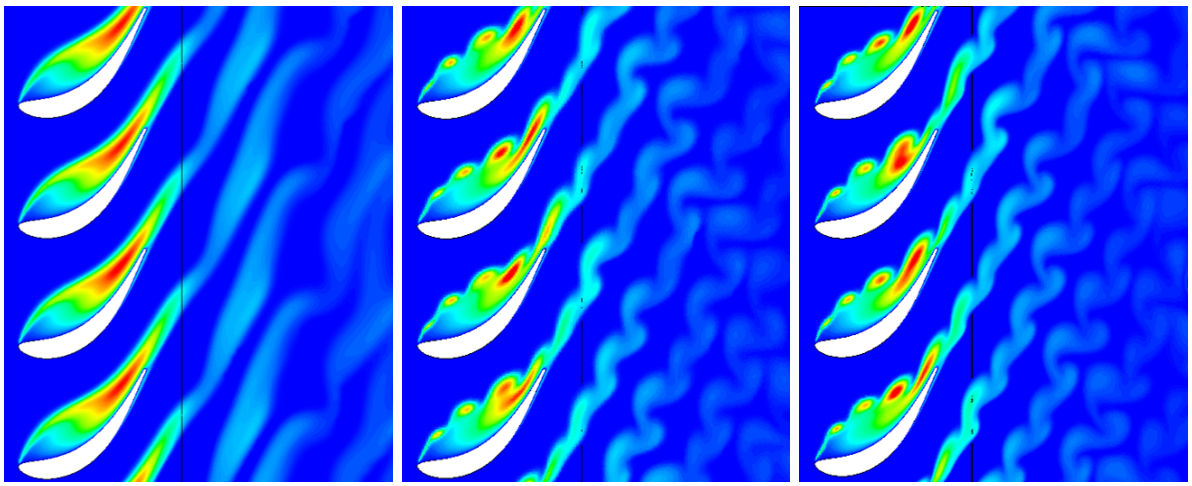

Figure 4.2: Contour of the turbulence kinetic energy for three different mesh sizes: coarse (left), medium (middle) and fine (right).

It is visually evident that the coarse mesh does not properly capture the wakes when comparing to the medium and fine mesh. The coarse mesh only manages to capture more general, large scale structures, while the medium mesh exhibits very similar flow structures as the fine mesh. Furthermore, table 4.1 shows key information regarding mesh quality and convergence for all three meshes.

Table 4.1: Comparison of simulation parameters and results

	Coarse	**Medium**	**Fine**
Cell size [mm]	0.4	0.2	0.1
Number of cells [-]	400 000	750 000	1 600 000
Time step size [s]	2e-5	1e-5	5e-6
Run time using 128 nodes [hours]	8	13	22
TA HTC at stag. point [W/m²K]	402.1	415.9	417.8
Stag. point HTC amplitude [W/m²K]	183	136	130
Avg. continuity residual [-]	1e-3	9.8e-4	8.2e-4

A closer look at the above table supports the observations made from the turbulence kinetic energy contours in figure 4.2. The stagnation point HTC clearly increases from the coarse mesh to the medium mesh, but changes only marginally for the fine mesh. Similarly, the amplitude of HTC fluctuations at the stagnation point decreases with mesh refinement in similar proportions, again showing only a small difference between the medium and fine meshes. The average continuity residual also decreases, while these being more similar between the different mesh sizes. The computation time is increasing approximately two-fold for each refinement of the mesh.

Considering these results, the medium mesh offers a good balance between accuracy and computational cost. It successfully captures the key flow phenomena of interest while significantly reducing the runtime compared to the fine mesh. Therefore, the medium mesh was selected for the remainder of the study.

Figures 4.3 to 4.5 show the medium mesh in detail, including the full computational domain and close-up views of the rotor blade and OGV. On average, the rotor blade trailing edge is resolved by approximately 10 cells across its diameter.

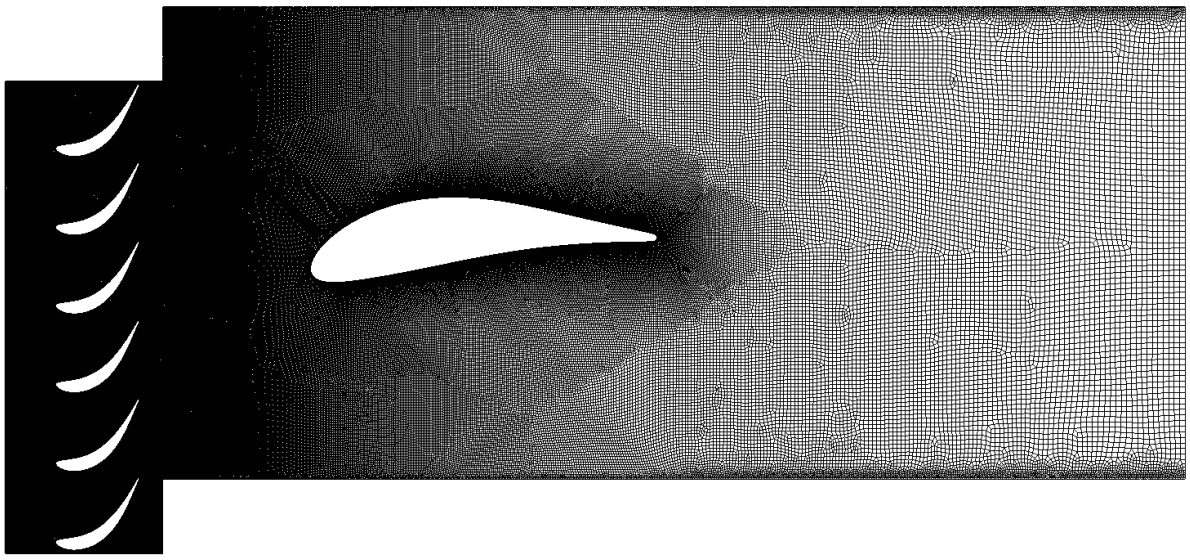

Figure 4.3: Medium mesh, including rotor and OGV domain.

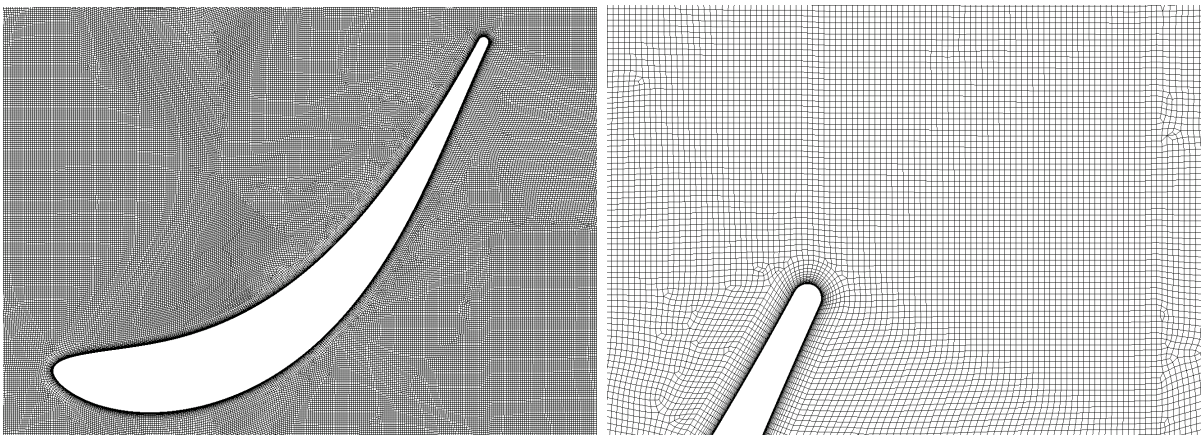

Figure 4.4: Close-up on one rotor blade (left) and rotor blade trailing edge (right).

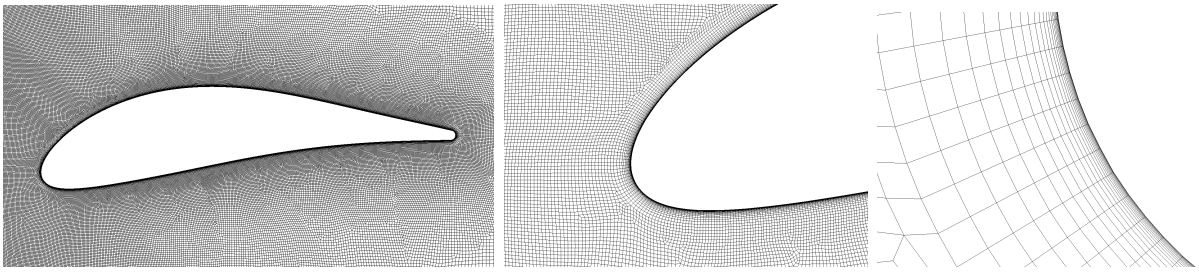

Figure 4.5: Close-up on the OGV (left), leading edge (middle) and leading edge boundary layers (right).

4.3 Steady-State Simulations

The 2D steady model developed during this thesis is compared to the 3D steady model from Murali's previous work at GKN. The 3D model is cut at the same midspan as the 2D model to allow for direct comparison.

Before comparing these two models, the HTC and velocity magnitude contour only from the newly developed 2D steady model is shown in figure 4.6. It can be seen that the HTC is at its highest at the OGV stagnation point where the flow is impinged. The HTC then decreases until transition to a turbulent boundary layer is achieved, which results in a local HTC peak in the aft. The flow accelerates strongly on the suction side, delaying the point of transition compared to the pressure side. Conversely, the transition on the pressure side occurs earlier although weaker.

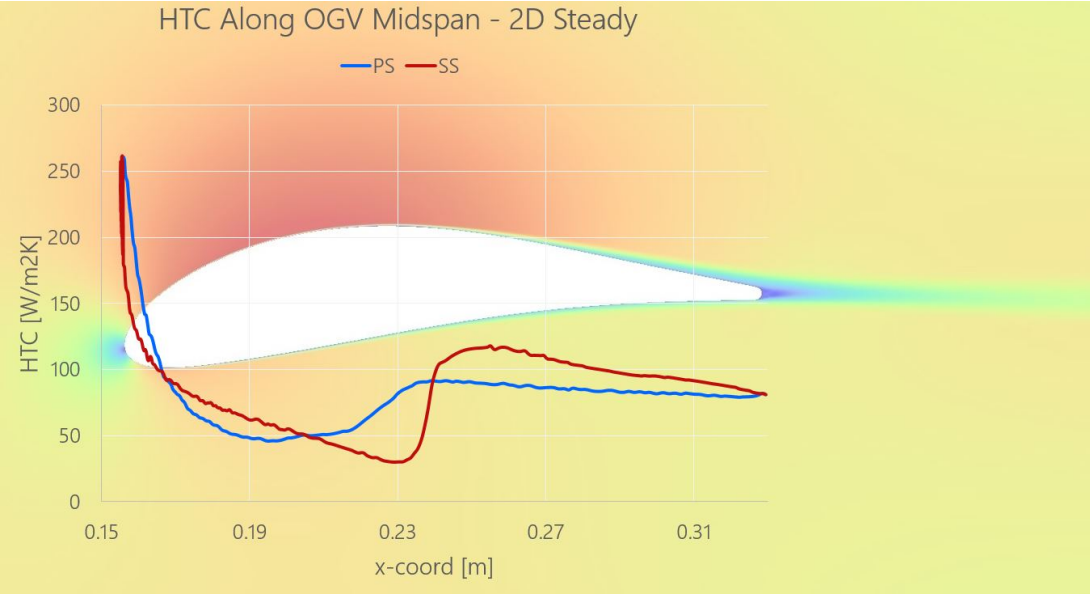

Figure 4.6: HTC-plot overlaid on velocity contour, 2D steady model.

4.3.1 Comparison between 3D and 2D steady models

The contours and plots in figures 4.7 to 4.10 show various contours from the previously developed 3D steady model and the newly developed 2D steady model. This comparison is done to establish how 3D effects play a role in HTC prediction.

As can be seen in figure 4.7, the velocity magnitude contours are very similar with flow impingement at the stagnation point followed by a strong acceleration on the suction side. Downstream of the OGV the velocity is slightly higher in the 3D model.

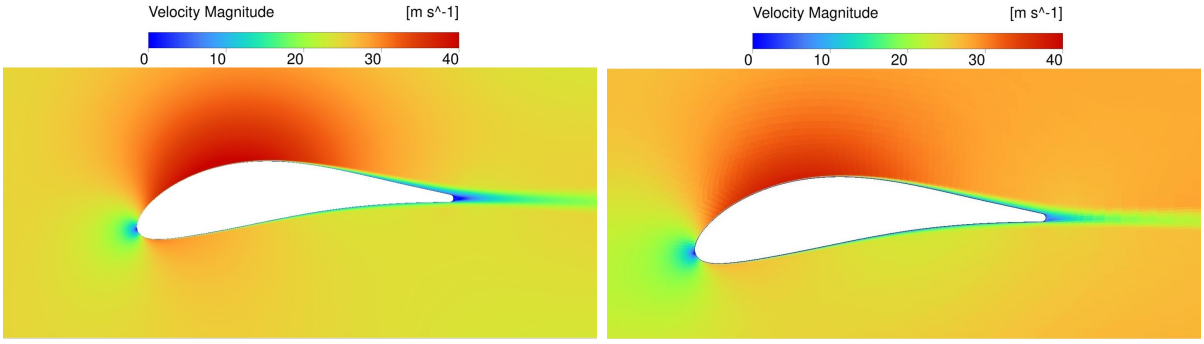

Figure 4.7: Velocity magnitude contours, 2D steady (left) vs 3D steady (right).

The turbulence kinetic energy is shown in figure 4.8. The two models show similar levels upstream of the OGV while it is slightly more prominent in the wake region for the 3D model.

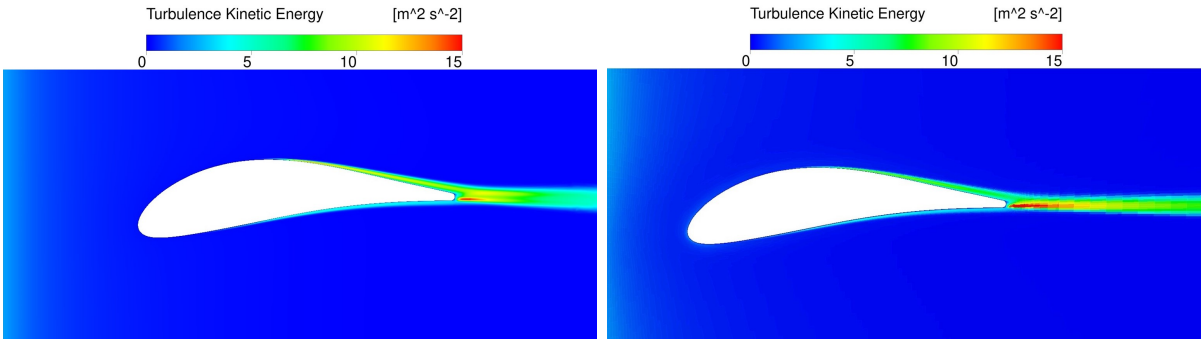

Figure 4.8: Turbulence kinetic energy contours, 2D steady (left) vs 3D steady (right).

Figure 4.9 shows the turbulence eddy dissipation. While the dissipation is higher upstream for the 3D model, it remains higher still downstream compared to the 2D model. This could be due to the reduction from three to two dimensions which might not allow for realistic and natural dissipation levels.

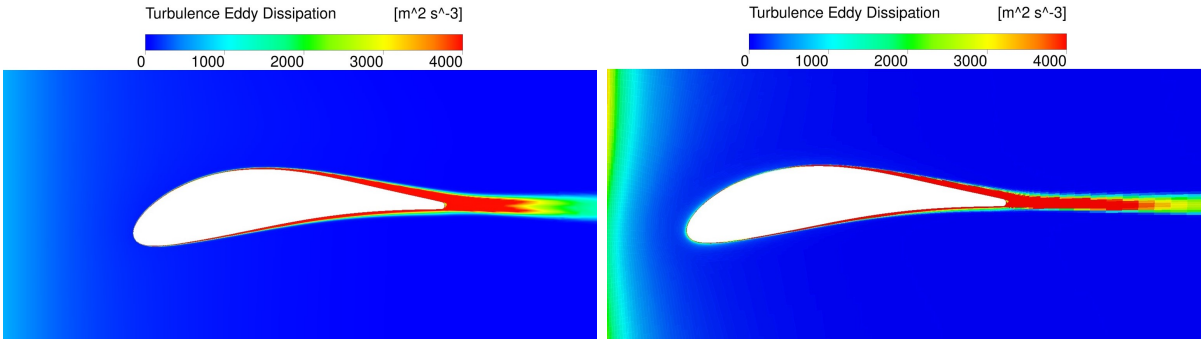

Figure 4.9: Turbulence eddy dissipation contours, 2D steady (left) vs 3D steady (right).

Finally, the HTC-profiles for the two cases can be seen in figure 4.10. It is clear that the HTC magnitude after the transition point is very similar for both models. However, in the laminar and transition regions there are significant differences, both in magnitude and point of transition. The 2D model has a stronger transition on both the pressure and suction side, but it is also delayed compared to the 3D model.

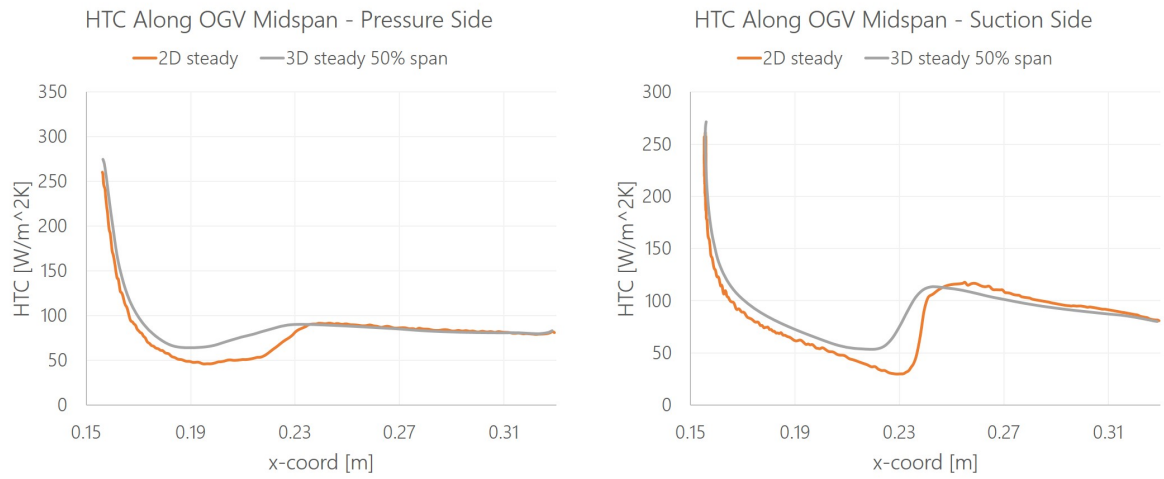

Figure 4.10: HTC plots for the pressure side (left) and suction side (right), 2D steady vs 3D steady.

4.4 Transient Simulations

Note that velocity and turbulence kinetic energy contours are presented in both instantaneous and time-averaged quantities. This is done to visualize the transient model's ability to capture unsteady flow phenomena while also providing averaged data to be evaluated and compared with the steady models. However, all other contours are only shown in their time-averaged form.

Figure 4.11 presents an instantaneous velocity magnitude contour in the stationary frame of reference. Rotor wakes are clearly identifiable as narrow bands impinging on the OGV leading edge. These wakes result in localized disturbances and varying flow acceleration along the suction side, affecting transition and unsteady boundary layer behavior.

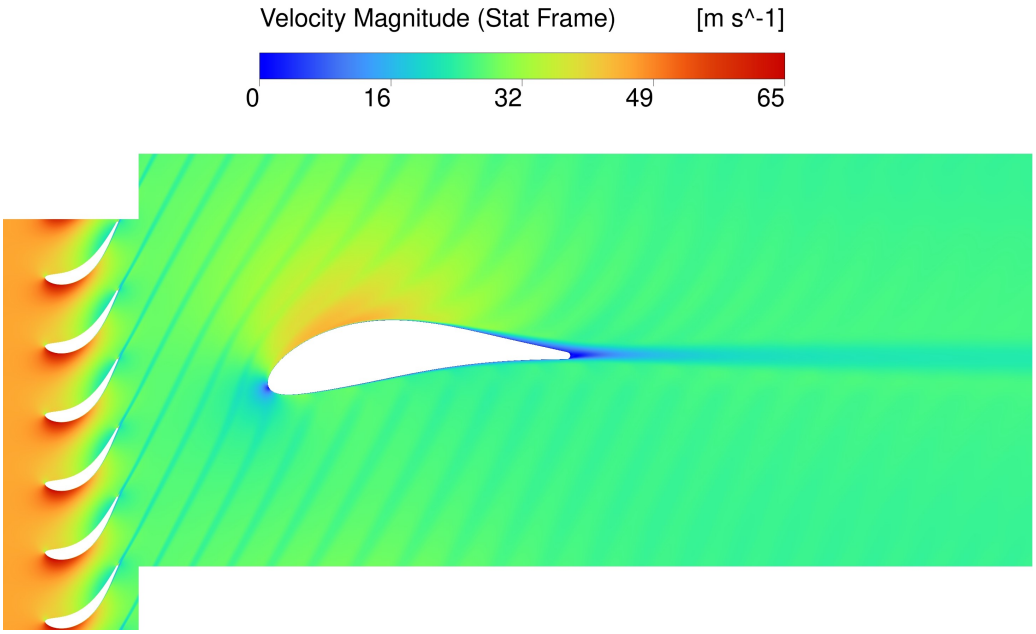

Figure 4.11: Instantaneous velocity magnitude, transient model

In contrast, the time-averaged velocity field in figure 4.12 shows a smooth flow structure in the OGV domain. The rotor-induced wakes are now averaged out and an even velocity profile can be seen at the OGV inlet.

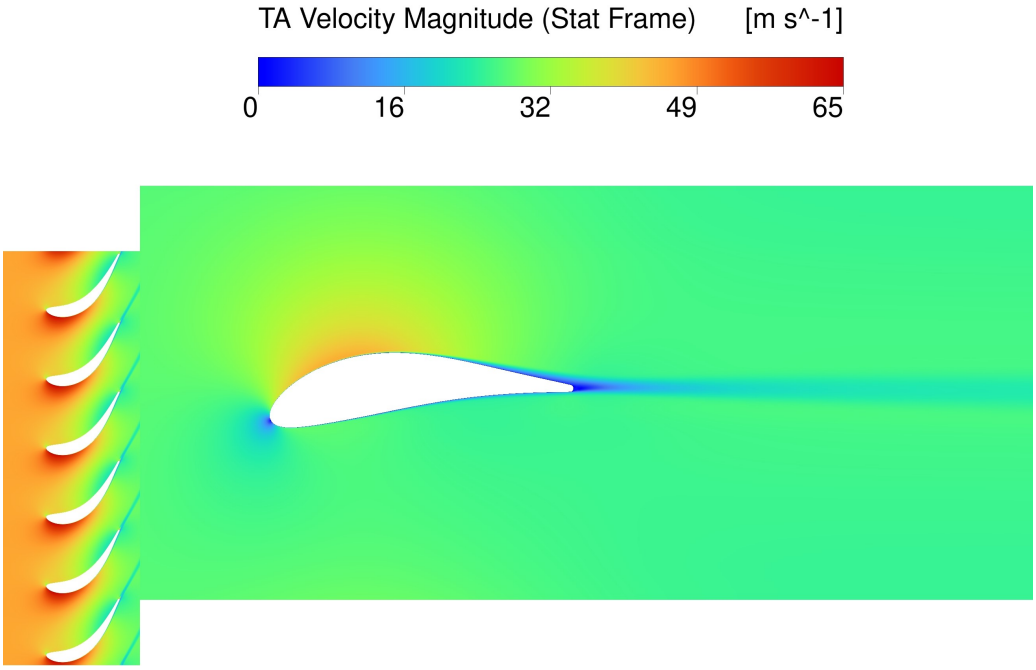

Figure 4.12: Time-Averaged velocity magnitude, transient model

The turbulence kinetic energy is displayed in figure 4.13. The general flow behaviour with the rotor wakes impinging on the OGV is clearly visible here too, as in the velocity magnitude contour.

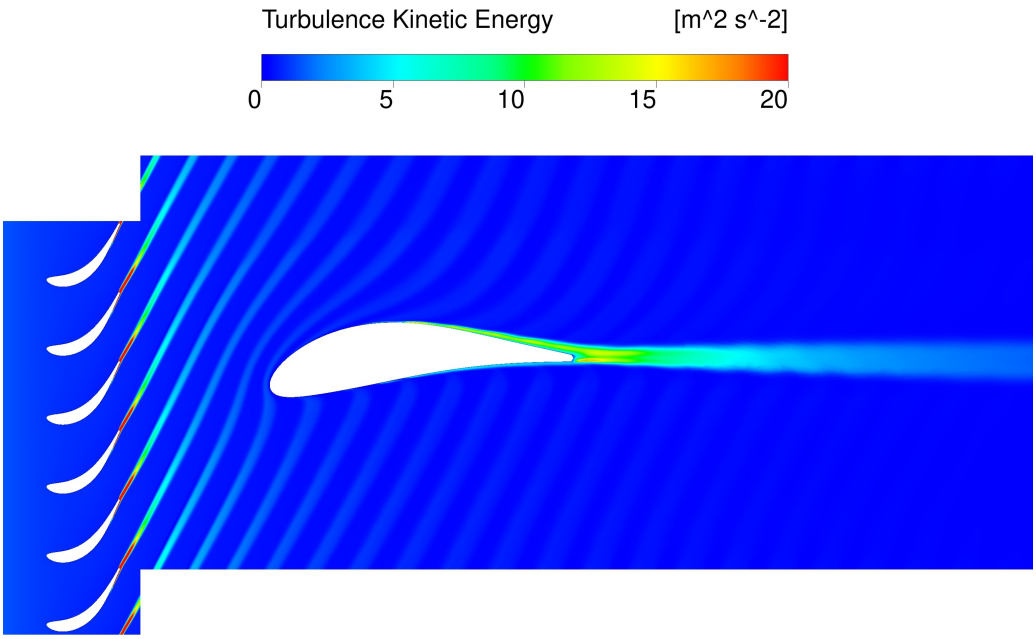

Figure 4.13: Instantaneous turbulence kinetic energy, transient model.

The time-averaged turbulence kinetic energy can be seen in figure 4.14. While the instantaneous contour shows high turbulence kinetic energy in local regions along the OGV inlet, the average profile is significantly lower. Much of the turbulence kinetic energy has dissipated when reaching the OGV leading edge.

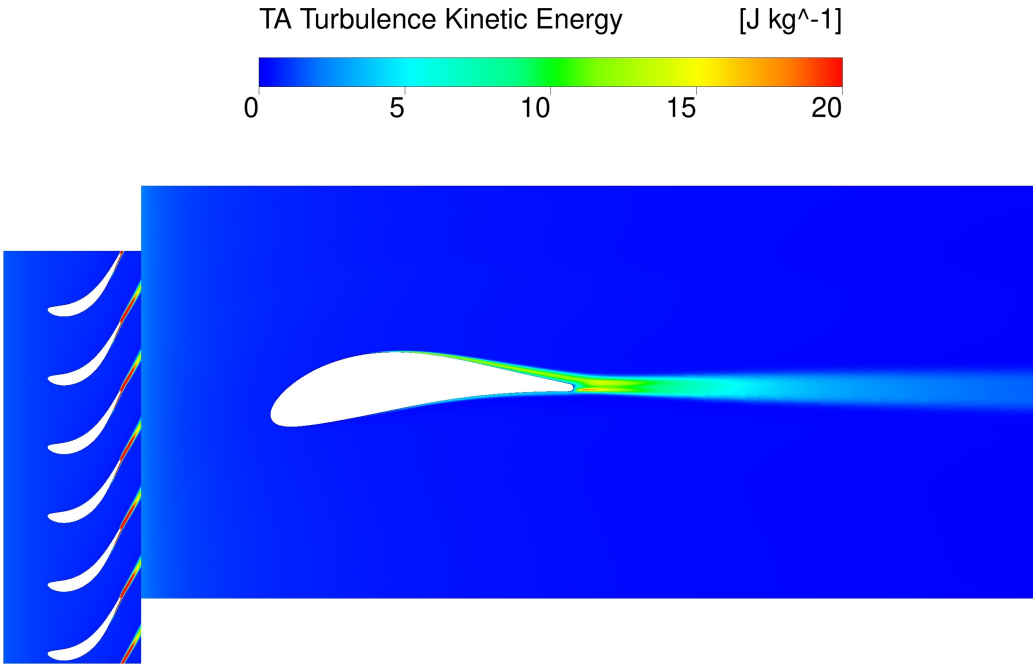

Figure 4.14: Time-Averaged turbulence kinetic energy, transient model.

Moving on, the time-averaged turbulence dissipation rate is shown in figure 4.15. Elevated

levels can be seen at the rotor trailing edge region and and along the OGV suction side aft, indicating strong turbulent mixing and heat transfer.

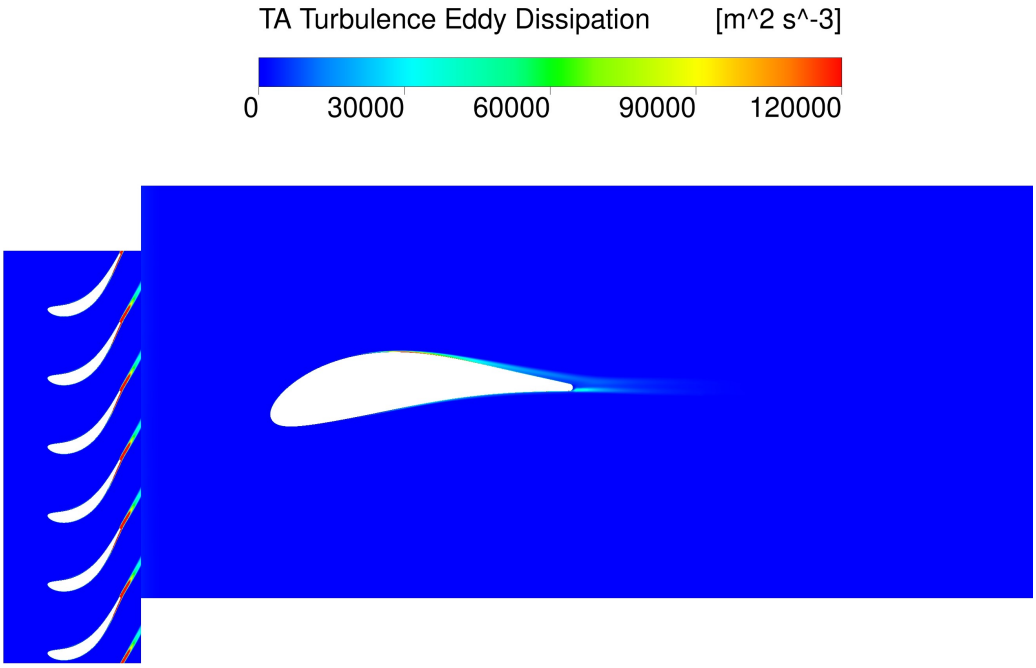

Figure 4.15: Time-Averaged turbulence eddy dissipation, transient model.

The time-averaged eddy viscosity ratio is displayed in figure 4.16. The maximum viscosity ratio is approximately 450 (although the contour range is only up to 130 for visual purposes) which is within reasonable ranges for transitional boundary layers and does not lead to so called "honey spots" with unrealistically high eddy viscosities.

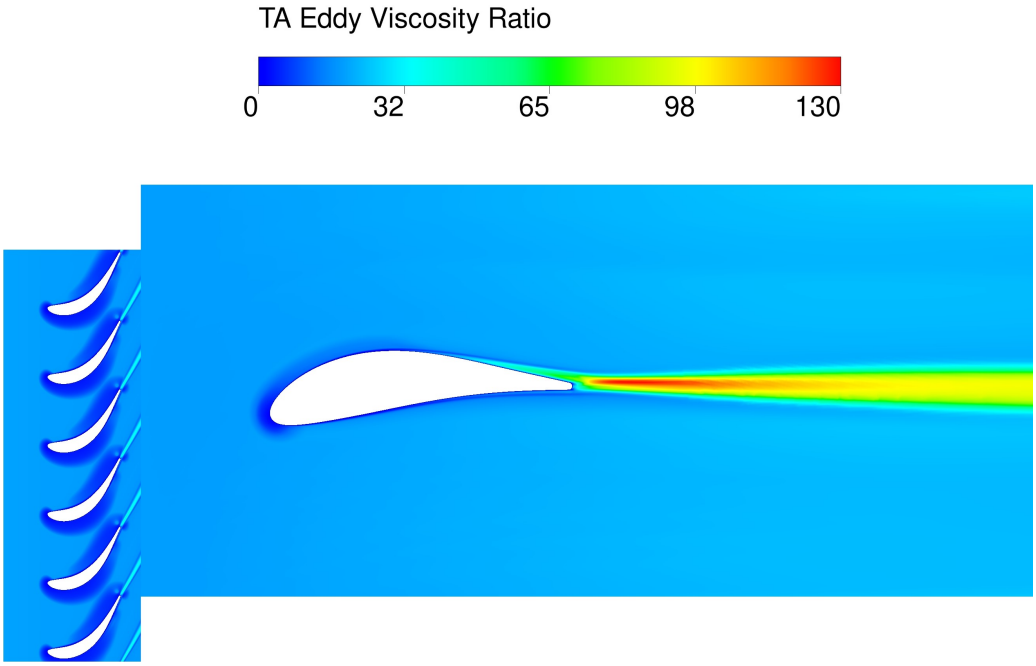

Figure 4.16: Time-Averaged eddy viscosity ratio, transient model.

Finally, figure 4.17 shows the HTC along the OGV midspan profile in the foreground with the velocity contour in the background. The rotor domain is excluded to place focus on the OGV only. Similar to the steady model, the maximum HTC is located at the stagnation point, quickly decreasing on both the pressure and suction sides until transition occurs.

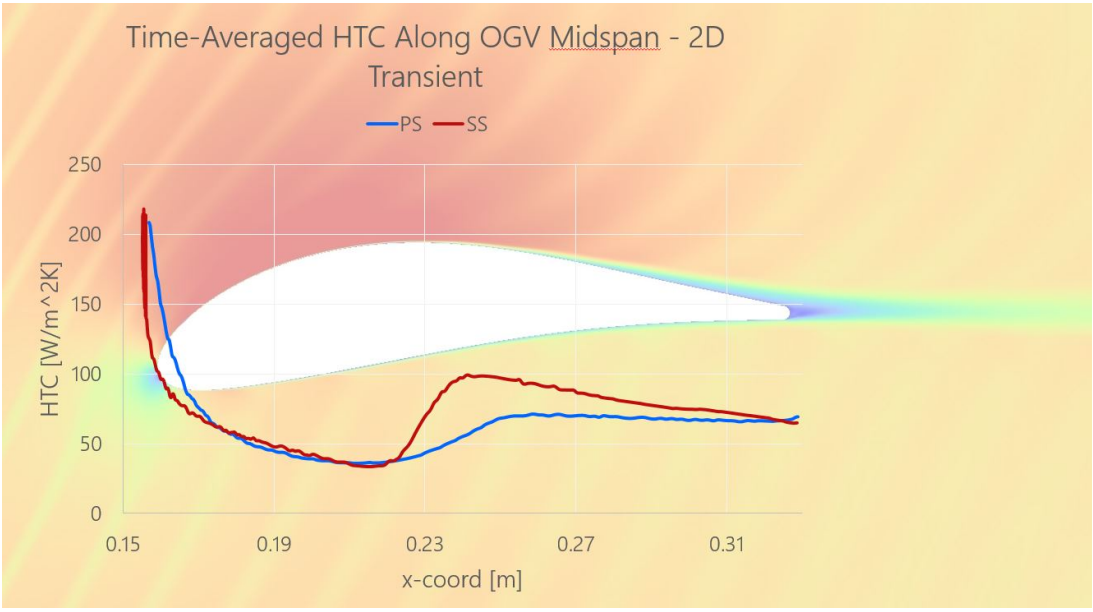

Figure 4.17: HTC-plot overlaid on velocity contour, transient model.

4.4.1 Temporal HTC Fluctuations

Figure 4.18 shows the temporal HTC variation at the OGV stagnation point. The HTC exhibits periodic behaviour in the form of two different frequencies in superposition. The high-frequency oscillations are consistent with rapid, periodic disturbances induced by blade wake impingement caused by the upstream rotors. Superimposed on this is a lower-frequency envelope, where a modulation pattern repeats every six high-frequency cycles. This arises from the modeled 30 degree sector which includes six rotor blades and a single OGV. As each rotor blade passes the stationary OGV, it induces one high-frequency disturbance. Since the OGV is fixed in space, it requires all six blades to pass before the wake interaction pattern fully repeats at that point. Thus, the low-frequency component reflects the periodic recurrence of the complete rotor wake pattern once per rotor revolution.

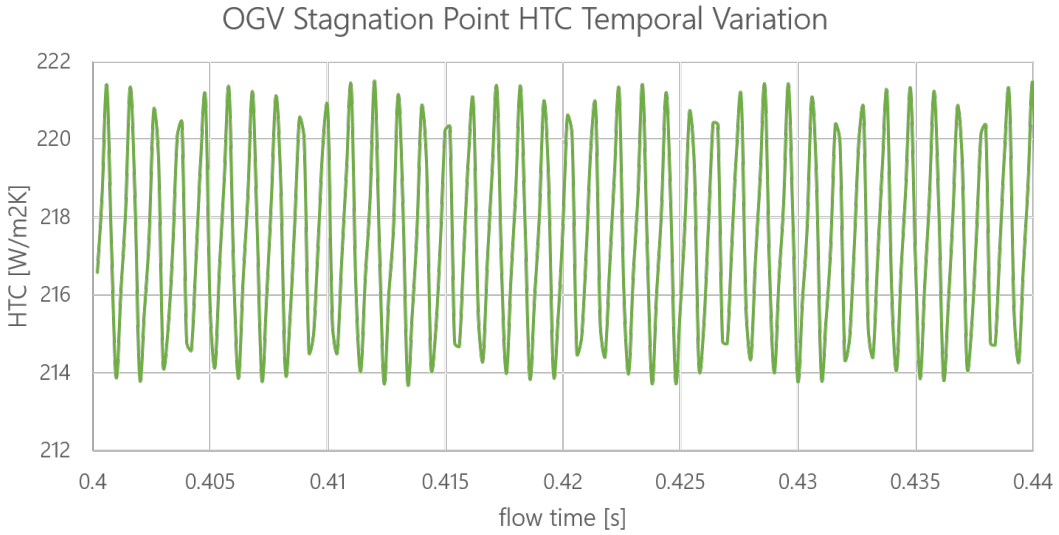

Figure 4.18: Temporal HTC fluctuations at stagnation point, transient model.

The upcoming figures show the HTC profile along the OGV for two different time steps: one where the stagnation point HTC is at its maximum, and the other at its minimum. The HTC plots are overlayed with a contour of the turbulence kinetic energy at the corresponding time stamp. Note that the range of the turbulence kinetic energy level has been decreased to accentuate variations along the OGV. Figure 4.19 shows the case with maximum stagnation point HTC and figure 4.20 shows the minimum.

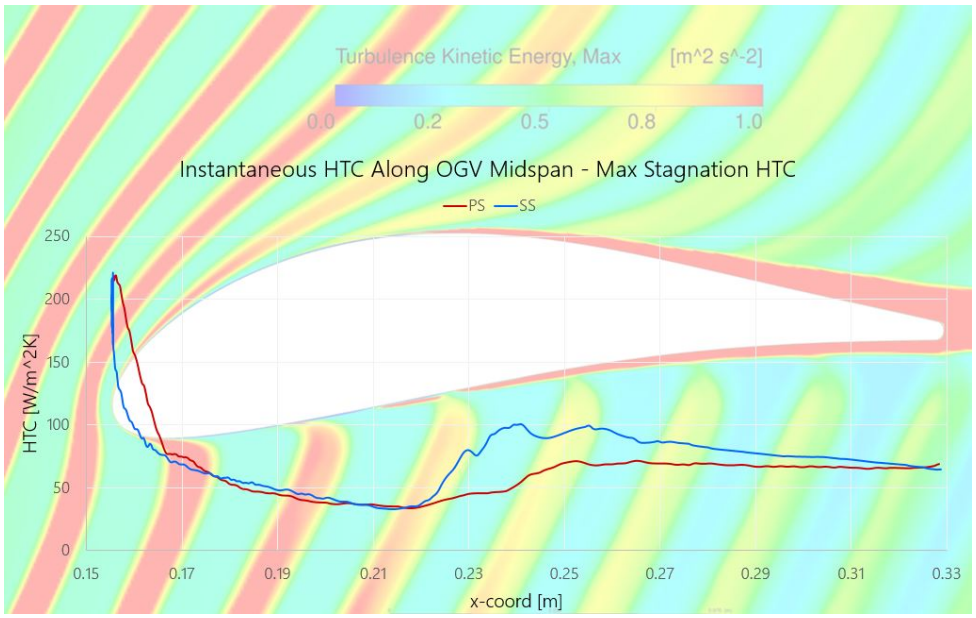

Figure 4.19: Instantaneous HTC-plot overlaid on turbulence kinetic energy contour, at maximum stagnation point HTC.

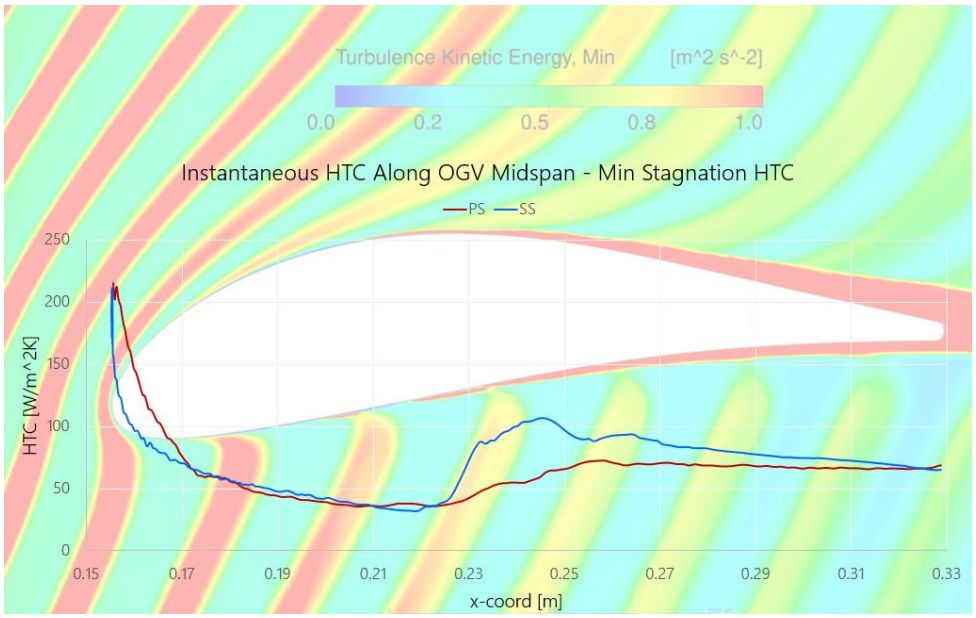

Figure 4.20: Instantaneous HTC-plot overlaid on turbulence kinetic energy contour, at minimum stagnation point HTC.

It is clear that the HTC peaks at the stagnation point when the leading edge is completely enveloped in the high turbulence kinetic energy field, and is at its lowest just before the high energy field reaches the leading edge. Furthermore, it can be seen in both these figures that the boundary layer is disrupted in small bursts, with several local HTC peaks most notable in the aft. This is attributed to the variations in the flow from the upstream wakes generated by the rotors, affecting the boundary layer periodically while it travels along the surface.

4.5 Comparison Between Various CFD Models and Experimental Data

To evaluate how much transient phenomena affect the HTC along the OGV, the 2D steady model is first compared to the transient model. HTC sensitivity for different turbulence quantities is then investigated for the 2D steady model. Following this, the results from the transient model is evaluated against experimental data from the CTR. Finally, a full comparison between all cases - that is, 3D steady-state vs 2D steady-state vs 2D transient vs CTR experimental data - is done.

4.5.1 2D Steady-State vs Transient

Note that only the OGV domain is included in the contours for the transient model to improve clarity and readability of the results.

When looking at the velocity contours in figure 4.21, the transient model captures flow fluctuations and upstream flow behaviour from the rotor blades. This is not the case for the steady model which only consists of the OGV domain and thus cannot capture upstream effects.

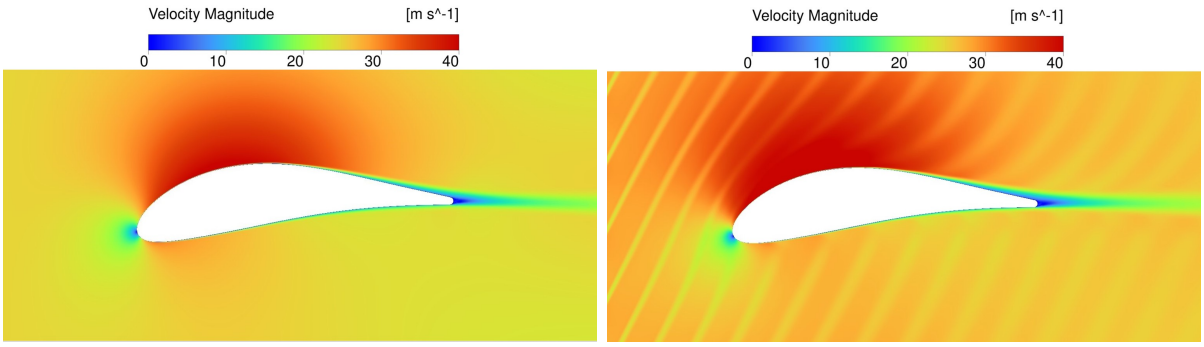

Figure 4.21: Velocity magnitude contours, 2D steady (left) vs transient (right).

However, when looking at the time-averaged velocity contour in figure 4.22, the general flow characteristics are similar between the two models. They both show impingement on the stagnation point and strong acceleration on the suction side followed by a streamlined wake downstream of the OGV. The velocity magnitude around in the free-stream is slightly higher for the time-averaged transient model compared to the steady model.

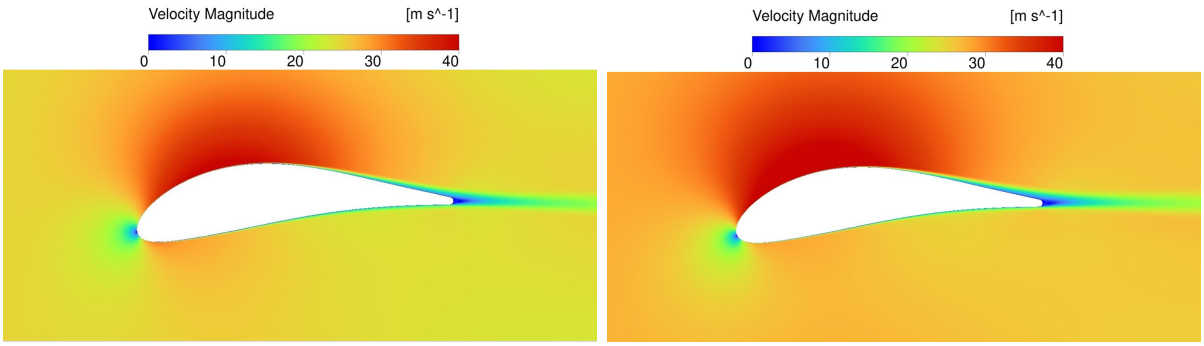

Figure 4.22: Velocity magnitude contours, 2D steady (left) vs time-averaged transient (right).

Figure 4.23 shows the turbulence kinetic energy for the two models. The transient case (time-averaged) displays somewhat higher turbulence kinetic energy downstream of the OGV. Both models show identical HTCs at the OGV inlet.

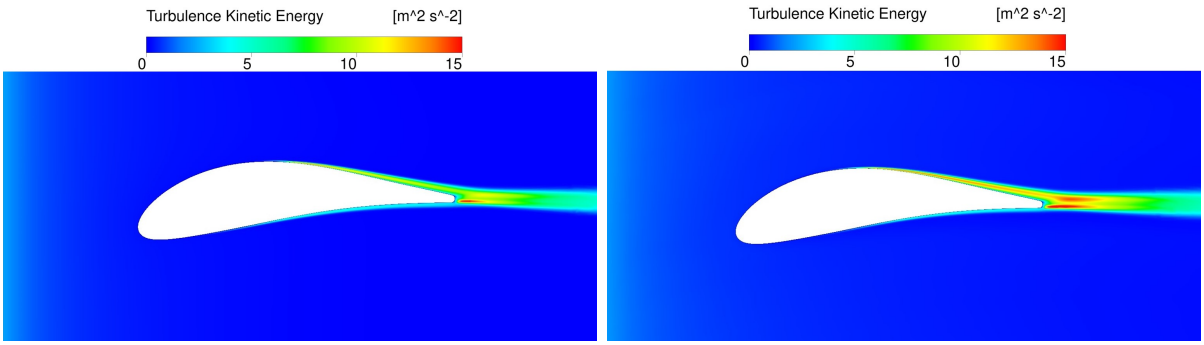

Figure 4.23: Turbulence kinetic energy contours, 2D steady (left) vs time-averaged transient (right).

Furthermore, the eddy dissipation is shown in figure 4.24. It is evident that the transient model has significantly higher dissipation at the OGV inlet. This is handled further under section 4.5.1.1.

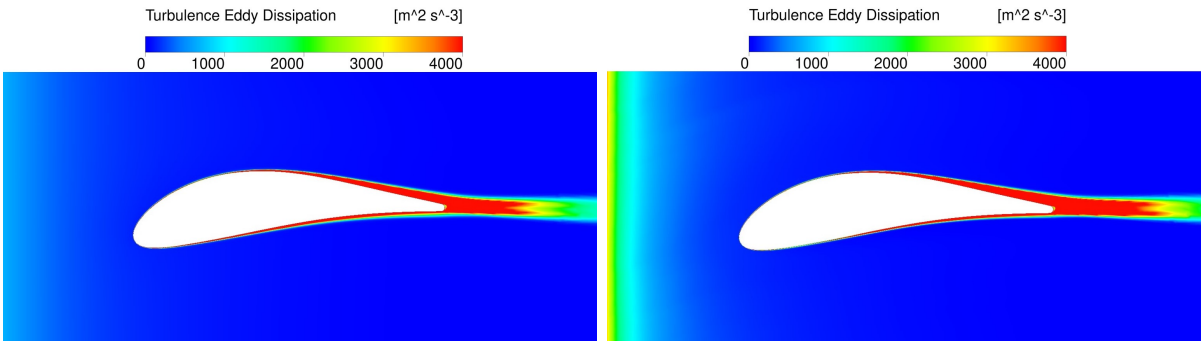

Figure 4.24: Turbulence eddy dissipation contours, 2D steady (left) vs time-averaged transient (right).

The plots in figure 4.25 show the HTC for the steady and transient cases for the pressure and suction side of the OGV. The HTC for the transient case is lower at all locations if taking the point of transition into consideration. However, the overall HTC shape distribution is similar between the two cases. For the pressure side, the transient model exhibits less significant transition and occurs later than the steady model. On the other hand, on the suction side the transient model predicts an earlier transition than the steady model, but still with a lower HTC.

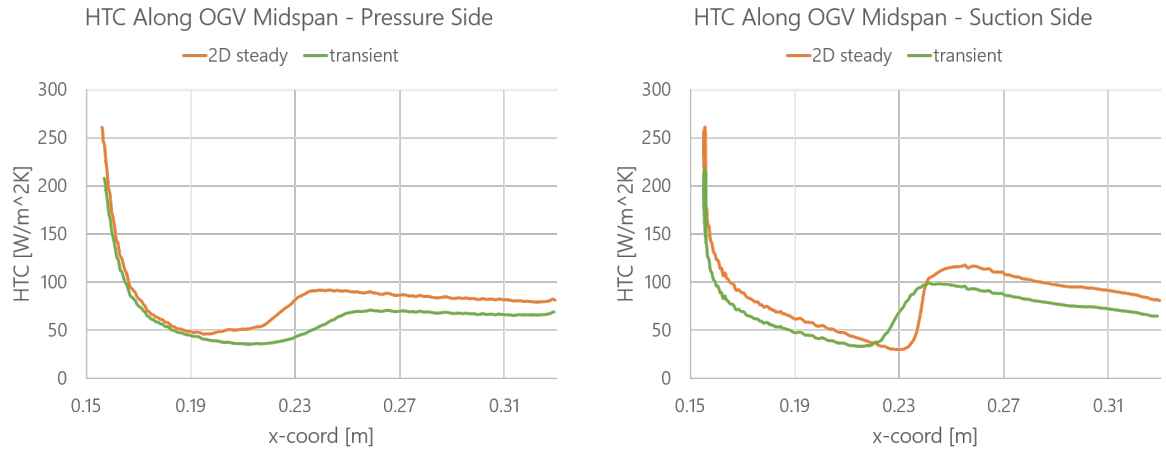

Figure 4.25: HTC plots for the pressure side (left) and suction side (right), 2D steady vs time-averaged transient

4.5.1.1 Matching Turbulence Quantities

Table 4.2 shows the velocity components and turbulence quantities at the OGV inlet for the steady and transient model.

Table 4.2: Velocity and turbulence quantities at OGV inlet, 2D steady vs time-averaged transient

	Transient	**2D steady**	**Difference**
Velocity magnitude [m/s]	27.1	25.0	+8 %
Velocity direction [deg]	-18	-17	+6 %
Turbulence kinetic energy [J/kg]	2.2	2.2	0 %
Turbulence eddy dissipation [m^2/s^3]	3596	703	+411 %

The magnitude and direction of the velocity is similar in both cases and considered to be within reasonable ranges. While the turbulence kinetic energy is identical up to one decimal point, the turbulence eddy dissipation is 411% higher in the transient case. This can also be seen in figure 4.26 which shows turbulence quantities from the OGV inlet to the OGV leading edge. At the leading edge, the steady model has turbulence kinetic energy levels of approximately 1.2 J/kg while the transient model has significantly lower levels of around 0.7 J/kg.

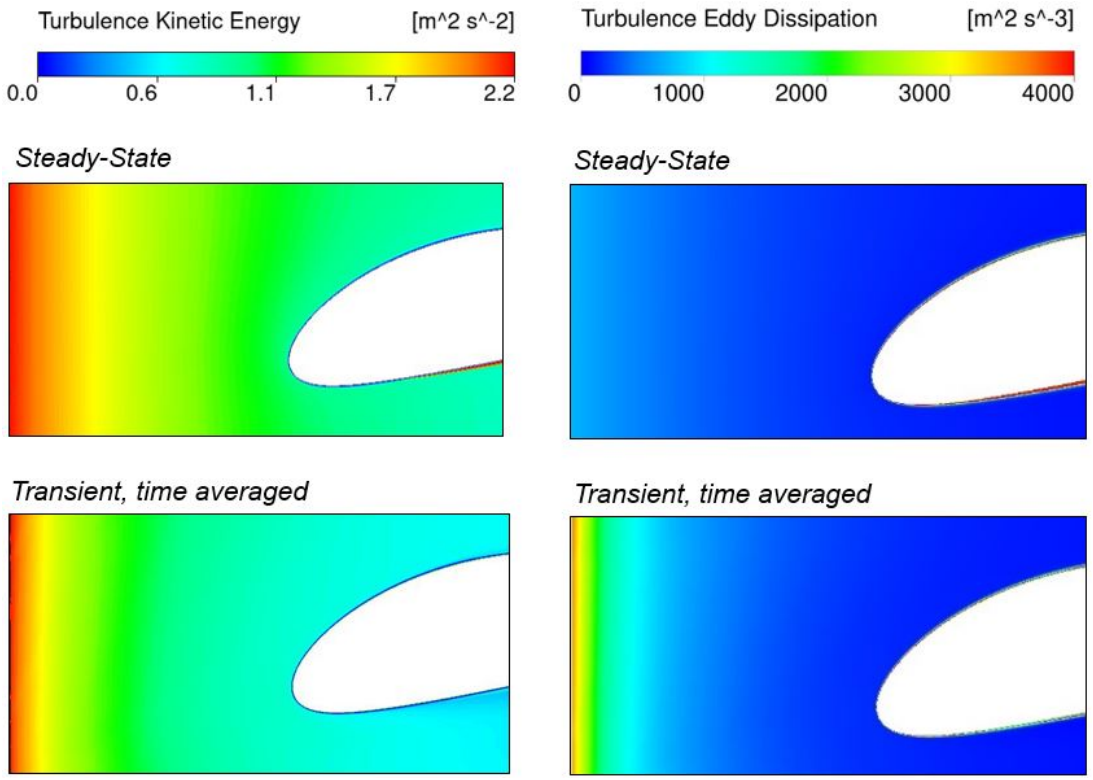

Figure 4.26: Turbulence kinetic energy contours (left) and eddy dissipation contours (right), 2D steady vs time-averaged transient - only including close-up from OGV inlet to OGV leading edge.

To further evaluate the effect of turbulence, the steady model was run using the turbulence quantities extracted from the transient model (that is, with higher dissipation). The turbulence kinetic energy for the two different steady simulations can be seen in figure 4.27.

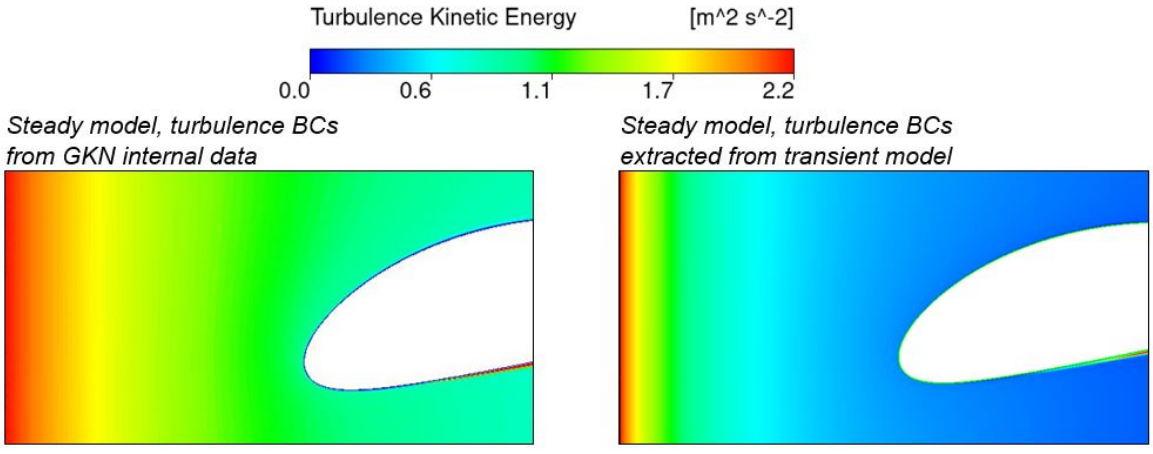

Figure 4.27: Turbulence kinetic energy contours, 2D steady using different turbulence boundary conditions - only including close-up from OGV inlet to OGV leading edge.

For the steady model with boundary conditions from the transient model, the turbulence

kinetic energy has now dissipated to significantly lower levels than in the previous simulation - in fact, even lower than the transient case. However, as can be seen in figure 4.28, the HTC profile is still almost identical for these two steady models. The only difference that can be seen in HTC magnitude is at the transition region, but even here the variation can be considered insignificant in relation to the strong increase in dissipation.

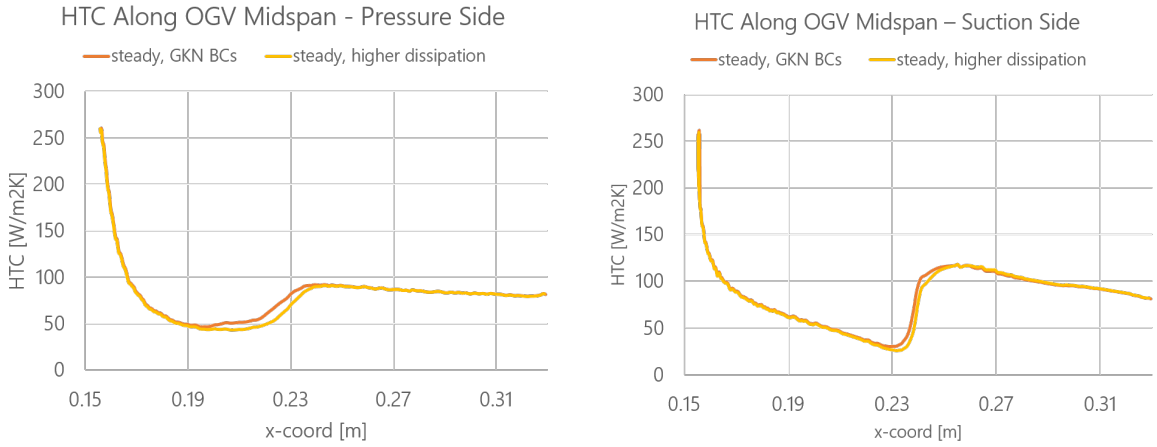

Figure 4.28: HTC plots for the pressure side (left) and suction side (right), 2D steady using different turbulence boundary conditions.

4.5.2 Transient Model vs Experimental Data

The experimental data from the CTR is only available for specific sections of the OGV, excluding the leading and trailing edge. This data has been matched with the CFD results such that the OGV profile coordinates are matched despite the missing experimental data in the leading and trailing edge regions.

Figure 4.29 shows the HTC from the transient model and the CTR data with results extracted at 50% span for the suction side and 48% for the pressure side (due to thermal couples placed at the pressure side midspan, thus preventing measurements from being taken). The transient model consistently under-predicts the HTC along the OGV for the available experimental data. The transition occurs later on the pressure side but earlier on the suction side, much like when comparing with the steady-state model. If looking at the transition peaks, the transient model's prediction of the HTC is 40% and 79% lower on the pressure and suction side, respectively.

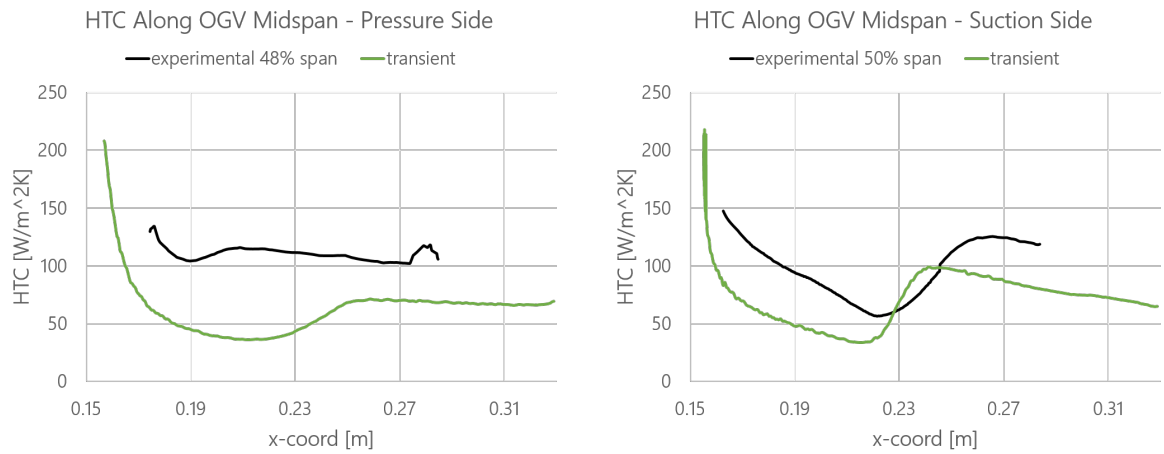

Figure 4.29: HTC plots for the pressure side (left) and suction side (right), transient vs CTR experimental data.

4.5.3 Final Comparative Analysis of All Cases

To conclude the comparative analysis, the HTC profiles for all CFD models - 3D steady, 2D steady, and 2D transient - as well as the experimental data are presented in figures 4.30 and 4.31. The 3D model predicts HTC levels most similar to the experimental data. Out of the 2D models, the steady model predicts more accurate HTC values as compared to the transient model. The transition point is best captured by the 3D model and 2D model for the pressure side and suction side, respectively. When comparing the point of fully completed transition, all CFD models predict later transition than the experimental data for the pressure side, while they all predict earlier transition for the suction side.

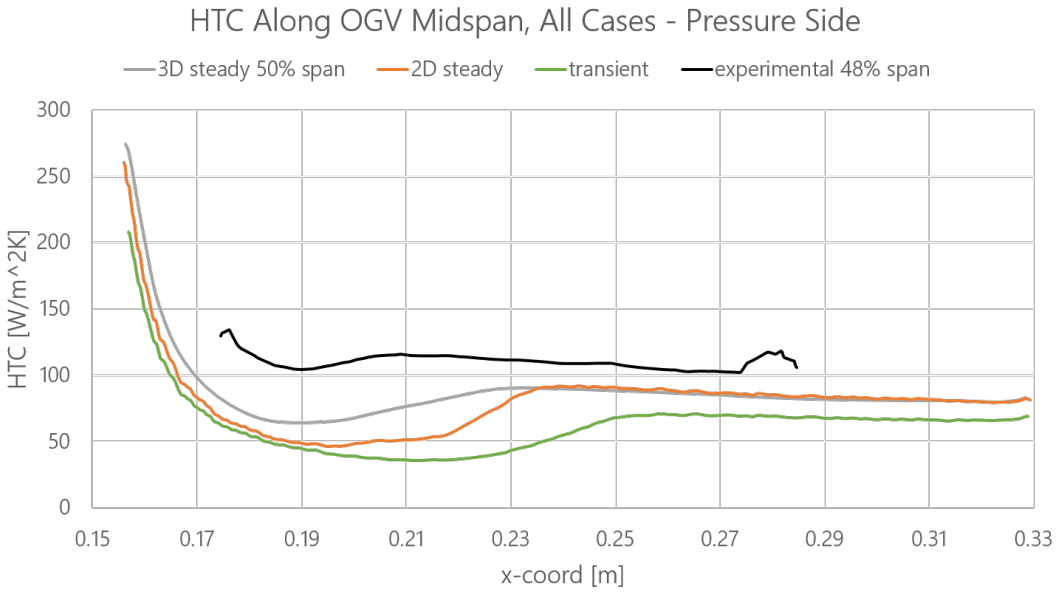

Figure 4.30: HTC plot for the pressure side, transient vs 2D steady vs 3D steady vs CTR experimental data.

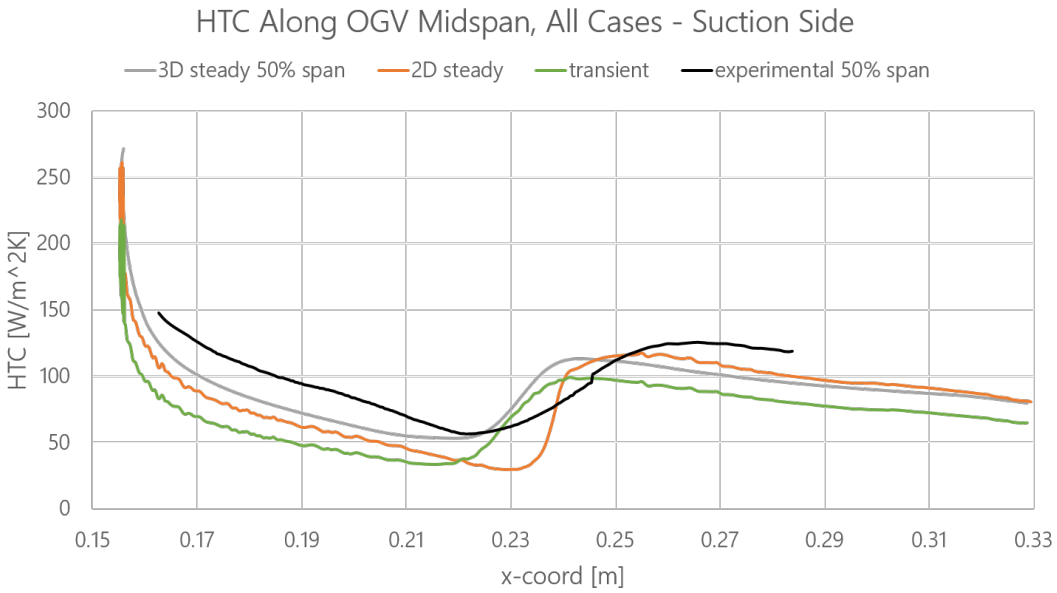

Figure 4.31: HTC plot for the suction side, transient vs 2D steady vs 3D steady vs CTR experimental data.

Finally, a table summarizing the main differences in HTC magnitude and transition location between the different cases is shown below.

Table 4.3: Comparison of key values for HTC and transition locations along the OGV.

	3D steady	**2D steady**	**Transient**	**CTR**
Stagnation point HTC [W/m^{2}K]	275	258	208	NA
Transition max HTC, PS [W/m^{2}K]	90	91	72	116
Transition max HTC, SS [W/m^{2}K]	113	116	99	125
Transition location, PS [%]	0.23	0.24	0.26	0.21
Transition location, SS [%]	0.24	0.25	0.24	0.26

5
Discussion

The work during this thesis has included several errors possibly affecting model accuracy and predictive reliability, including geometry resolution, mesh convergence, and the chosen turbulence modeling approach. Significant discrepancies between the transient and steady-state results, as well as differences observed when comparing numerical outcomes with experimental measurements, have left many questions and areas of investigation and improvement. The following discussion elaborates on these issues, including model comparisons and recommendations for enhancing model fidelity and guiding future improvements.

5.1 Effects of Geometry Quality

Although the lower geometry resolution did not significantly alter the overall magnitudes of the HTC when comparing results across different mesh densities, it notably introduced local irregularities such as noise and jagged profiles. These irregularities are most likely caused by stair-stepping artifacts resulting from inadequate geometric resolution, especially noticeable at the leading edges and curved surfaces of the blades. As previously highlighted in section 4.1, insufficient geometry quality leads to these discrete steps rather than smooth curves. It would be of interest to perform either a form of averaging or interpolation of the current geometry. An even better option would be to improve the source geometry or create a higher quality parasolid.

5.2 Reliability of Mesh Convergence Study

The mesh convergence study revealed that the medium-resolution mesh (cell edge size 2e-4m) was sufficient to resolve key features such as OGV heat transfer and wake development. The chosen mesh contains on average 10 cells across the rotor blade trailing edge which is the approximate number of cells required in order to sufficiently capture the wakes. While the mesh requirements will deviate from these findings when moving on to 3D modeling, the mesh convergence results from this thesis could still be used as a baseline to start from. The main requirement should be that the wakes from the rotors has to be maintained sufficiently up until the OGV. The fact that previous studies used much coarser meshes suggests that further improvements in model fidelity can still be achieved by refining mesh resolution, particularly in critical wake-, transition-, and separation zones.

However, it is worth pointing out that the mesh convergence study was done using the

incorrect inlet boundary conditions. This was due to an error when extracting the velocity components from the 1.5-stage model. The boundary conditions were corrected at a very late stage in the thesis, which deemed an updated convergence study implausible considering the remaining time. It was therefore decided to move on with the performed mesh study, and concluded that it still should yield similar mesh requirements as if correct boundary conditions would have been used.

The incorrect boundary conditions was more in line with off-design conditions, with a separated pressure side with vortices generated from the rotor leading edge. The wakes downstream of the rotor also exhibited much higher turbulence kinetic energy levels and larger turbulence structures compared to the case with correct boundary conditions. Considering that the chosen mesh was able to capture these stronger flow fluctuations and more unsteady behaviour, one could argue that the mesh requirements when using the correct boundary conditions should not exceed those when using incorrect boundary conditions. However, this cannot be explicitly concluded before an updated mesh convergence study is performed to confirm this.

5.3 Similarities Between 2D and 3D Models

The 2D steady-state model showed strong qualitative agreement with the 3D steady-state simulation at midspan. Both simulations captured the primary features of the HTC distribution, including the stagnation point peak and downstream transition behavior. The differences, particularly on the suction side, could be attributed to the absence of 3D secondary flows and span-wise velocity components in the 2D model.

Even though the 2D model is similar to the 3D model with slightly lower HTC predictions, the 2D model lacks the capability to simulate purge flow interactions, tip clearance effects, and end wall film cooling, which are inherently three-dimensional. As such, while the 2D steady-state model offers a computationally efficient alternative, its application should be limited to specific span investigations or preliminary design assessments.

5.4 Transient Model's HTC Under-Predictions

An unexpected yet important result from this study is that the 2D transient simulation, despite resolving more unsteady phenomena and displaying higher turbulence dissipation rates close to the OGV surface, results in a lower time-averaged HTC along the OGV compared to the steady-state model. This could be a result of multiple factors.

The absence of out-of-plane motion in 2D models restricts the physical realism of the turbulent structures. In 3D flows, wake vortices undergo complex stretching and breakup, which enhances mixing and thermal transport toward the wall. In 2D, this mechanism is missing. The dissipation measured in the transient simulation might reflect bulk energy decay rather than near-wall turbulent mixing, which is what actually drives the convective heat transfer. While the transient case shows higher turbulent dissipation, this only indicates that turbulence kinetic energy is being converted into thermal energy somewhere

in the flow — not necessarily at the wall. As can be seen when running the steady model with higher dissipation, the HTC still maintains at similar levels which suggests that there are other factors affecting these results.

The key parameter controlling HTC is the ability of turbulent eddies to disrupt the thermal boundary layer, which is not explicitly guaranteed by a high dissipation rate on the global scale of the simulation domain. However, turbulence dissipation alone is not a reliable predictor of wall heat transfer, especially in 2D URANS simulations. More broadly, this shows the potential importance of 3D modeling when studying wake-boundary layer interactions and unsteady heat transfer phenomena in turbine rear structures.

5.5 Effects of Unsteady Temporal Fluctuations

Naturally, the transient simulation - while not sufficiently capturing thermal behaviour - still manages to resolve the wakes and turbulence generated by the rotors. The onset of transition on the OGV suction side is slightly earlier in the transient case compared to the experimental data, while the pressure side instead experiences transitions later.

All three simulation models predicted similar points of transition. However, when looking at the instantaneous plots and contours under section 4.4, it is evident that unsteady effects from the upstream rotors cause fluctuations in the HTC and transition. When time-averaging these results the instantaneous fluctuations smooths out, resulting in overall HTC trends similar to the steady simulations. This suggests that while the transient model captures unsteady behaviour, it does not seem to seriously impact the HTC and transition on a larger time scale.

5.6 Future Work and Recommendations

Due to the inherent time limitations of this project, many interesting areas of investigation was left out and are included below for future work within the topic.

Performing updated mesh study: Given the fact that the mesh independence study included in this thesis was done using incorrect boundary conditions, a new study should be done to confirm whether or not the requirements changes with the adjusted inlet conditions. This should be done first of all, before moving on to any other further work.

Adding stator domain: Like previously mentioned, the stator domain upstream of the rotor domain was excluded to reduce complexity and computation time. Adding this stage would however affect the flow characteristics, naturally adding more flow fluctuations and gradients when interacting with the downstream components.

Developing a 3D transient model: Part of the results for this thesis was that 2D transient models might not be sufficient to capture the relevant flow phenomena to accurately measure the HTC in the TRS. Therefore a 3D model should be made and evaluate against the experimental data from the CTR. This would mean performing an updated

mesh convergence study since the flow behaviour is inherently different in 2D and 3D models. Much care would have to be taken in order to minimize the number of cells since the transient nature of the problem increases the computation time drastically. The belief is that much fewer cells in the span-wise direction is needed and its distribution can be modified depending on what is investigated. This model would also allow for further investigation into for example end wall HTCs, pocket/cavity flow behaviour and film cooling.

Improve geometry quality: It would be interesting to evaluate whether the jagged-ness of the geometry contributes to inaccurate predictions of the HTC or if simple reparations (eg interpolation) is a sufficient remedy.

Comparing on- and off-design conditions: So far, only on-design conditions have been evaluated. Using off-design conditions would lead to more severe flow fluctuations and higher turbulence which should affect both the HTC and transition. This comparison is highly relevant to evaluate the full engine operation cycle.

Use real engine operating conditions: When and if more accurate simulation models have been developed, it would be interesting to investigate how the thermal and aero characteristics looks like in the TRS when using actual engine operation conditions.

Difference when using transition vs fully turbulent turbulence model: As of now, GKN uses fully turbulent modelling when evaluating the HTC in the TRS as to not under-predict the HTC too severely. If more accurate models are developed, it would be relevant to compare the current fully turbulent model with a transition model to accurately capture the HTC along the full OGV profile.

Using temperature BC around OGV with varying temperature: In the CFD model, a constant temperature was set around the OGV. However, the CTR measures the surface temperature of the OGV nearly along the full span. Implementing this into the simulations should provide more accurate HTC predictions.

6
Conclusion

This study undertook a detailed transient CFD analysis to explore the effects of unsteady flow induced by rotor blade wakes on OGV heat transfer in the TRS. By comparing 2D transient simulations against experimental data and both 2D and 3D steady-state CFD models, it became evident that although the transient approach effectively revealed periodic and temporal variations that steady-state methods inherently miss, it consistently underpredicted overall HTC magnitudes.

This underprediction points to several limitations, notably the dimensional reduction from a realistic 3D geometry to a simplified 2D domain, which inherently excludes critical flow characteristics such as span-wise flow effects, secondary flow structures, and complex vortex shedding phenomena prevalent in turbomachinery applications. Furthermore, a new mesh study should be performed considering that incorrect boundary conditions were used during the current study. Updated requirements regarding the mesh could impact the results substantially.

Looking forward, evaluating the validity of a 3D transient CFD model would be of interest to investigate the differences in turbulence levels and HTC predictions. This is ideally coupled with more advanced turbulence modeling frameworks to better represent complex unsteady flows. Additional experimental validation under varied operating conditions, including both on-design and off-design scenarios, would further enhance the robustness and applicability of these CFD models.

In conclusion, while the transient simulations provided valuable qualitative insights into unsteady heat transfer behaviors, substantial quantitative improvements are required to draw further conclusions. Addressing these aspects should lead to improved and more accurate simulation models which assists in design decision-making as well as overall longevity in aero-engine components.

Bibliography

[1] Gustaver, M. (2020) A Chalmers University of Technology Master's thesis template for LaTeX. Unpublished.

[2] Vikhorev V, Jonsson I, Tokarev M et al (2022) Experimental study on the low-pressure turbine wake interaction and development in the turbine rear structure.

[3] Lowery GW, Vachon RI (1975) The effect of turbulence on heat transfer from heated cylinders

[4] Ames FE, Moffat RJ (1990) Heat transfer with high intensity, large scale turbulence: the flat plate turbulent boundary layer and the cylindrical stagnation point

[5] Wang G, Vanka PS (1995) Convective heat transfer in periodic wavy passages

[6] Scholten JW, Murray DB (1998) Unsteady heat transfer and velocity of a cylinder in cross flow—I. Low freestream turbulence

[7] Murali A (2023) The Numerical Investigation of Outlet Guide Vane Heat Transfer

[8] Dhanasegaran R (2018) Experimental and Computational Investigations of Heat Transfer in Aero Engine Outlet Guide Vane (OGV)

[9] Wang Z, Ireland PT, Jones TV (2016) An advanced method of processing liquid crystal video signals from transient heat transfer experiments

[10] Yang Y, Nikolaidis T, Jafari S, Pilidis P (2024) Gas turbine engine transient performance and heat transfer effect modelling: A comprehensive review, research challenges, and exploring the future

[11] Components of jet engines, Wikipedia. (Online). Available: $https://en.wikipedia.org/wiki/Components_of_jet_engines$.

[12] Vikhorev V, Nylander P, Chernoray VG, Larson J, Thulin O (2021) Experimental and Numerical Flow Analysis of an Engine-Realistic State-of-the-Art Turbine Rear Structure

[13] Lakshminarayana B (1996) Fluid Dynamics and Heat Transfer of Turbomachinery, 1st ed.

[14] Incropera FP, DeWitt DP, Bergman TL, and Lavine AS (2011) Fundamentals of Heat and Mass Transfer, 7th ed.

[15] Versteeg HK and Malalasekera W (2007) An Introduction to Computational Fluid Dynamics: The Finite Volume Method, 2nd ed.

A

Appendix 1

A.1 Sliding Mesh Setup Guide, 2D

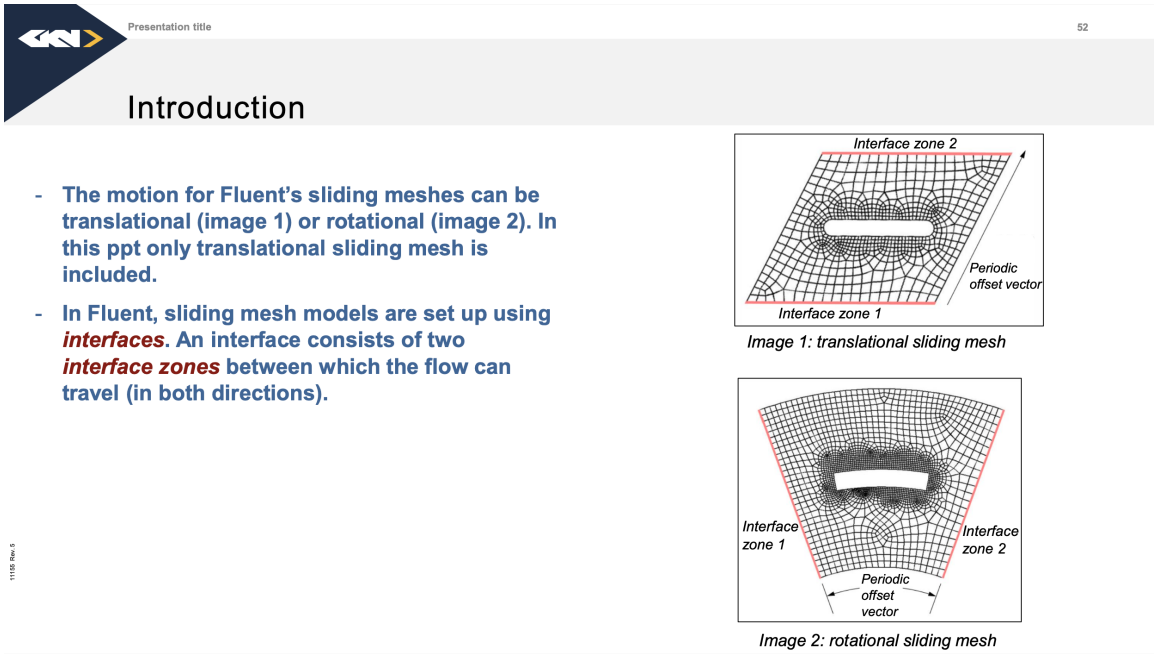

Figure A.1: Sliding mesh guide, part 1/9

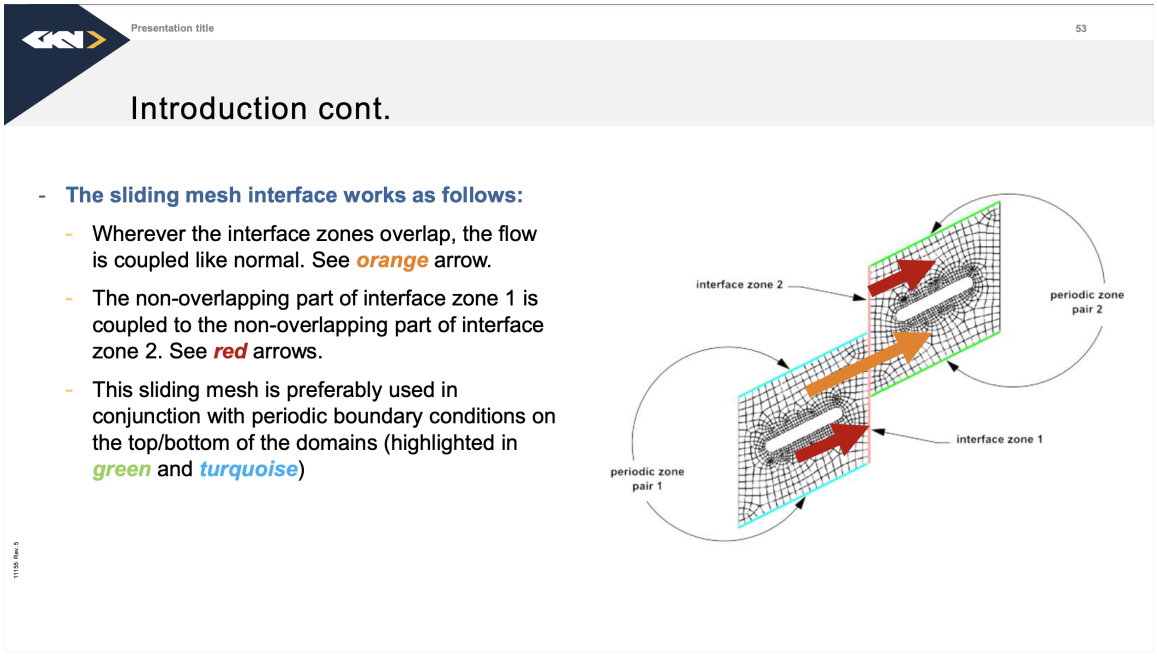

Figure A.2: Sliding mesh guide, part 2/9

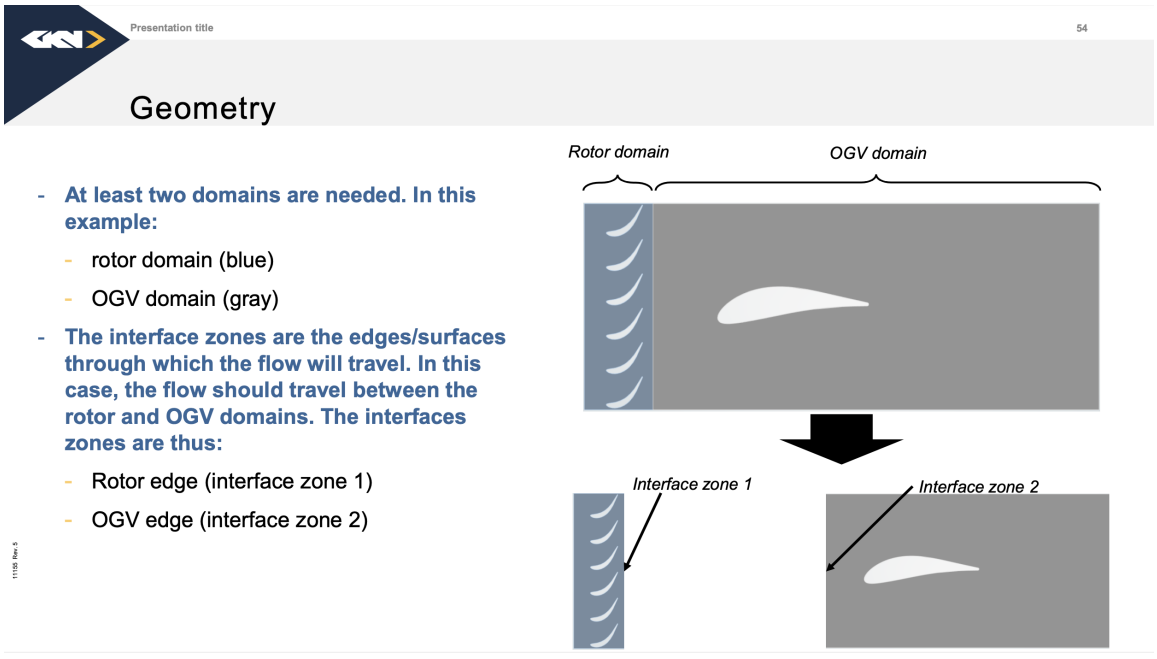

Figure A.3: Sliding mesh guide, part 3/9

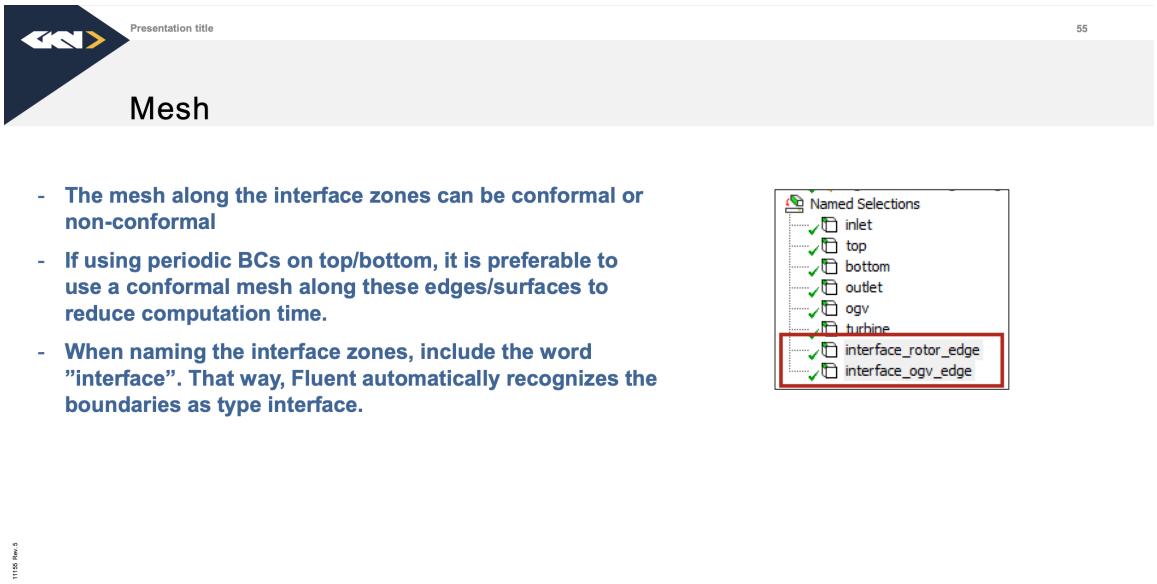

Figure A.4: Sliding mesh guide, part 4/9

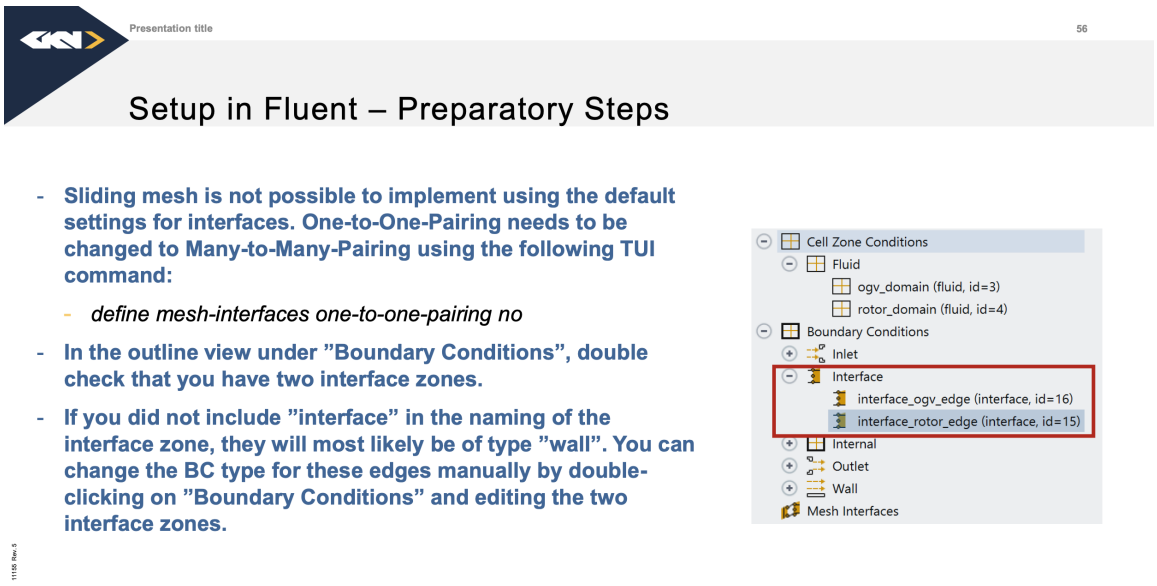

Figure A.5: Sliding mesh guide, part 5/9

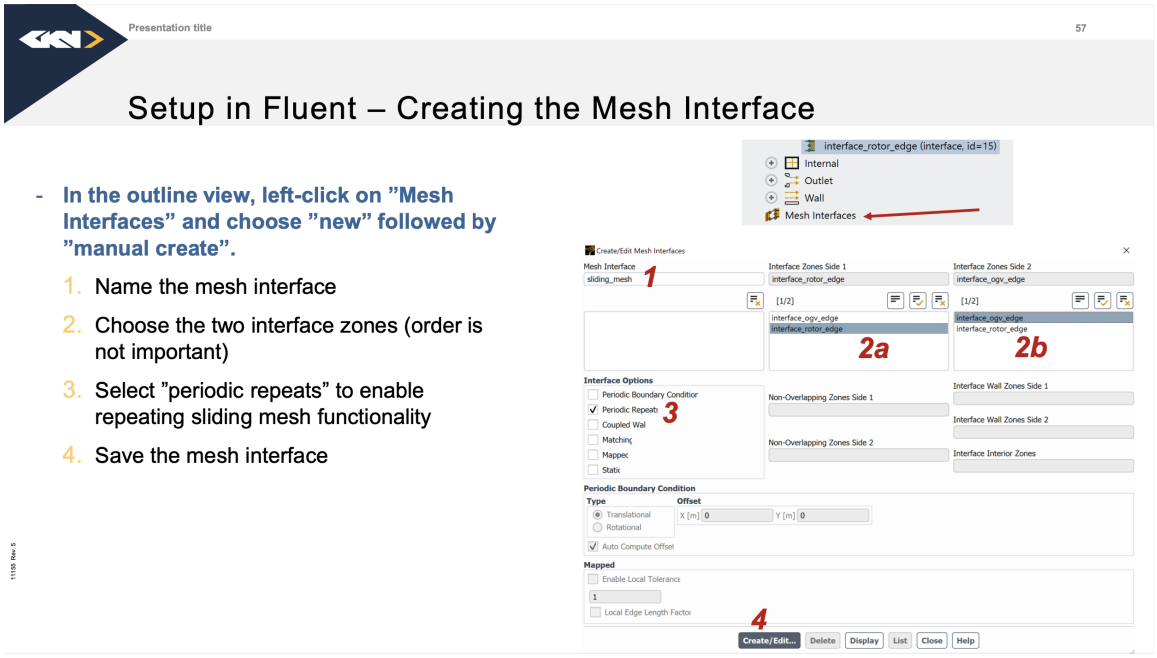

Figure A.6: Sliding mesh guide, part 6/9

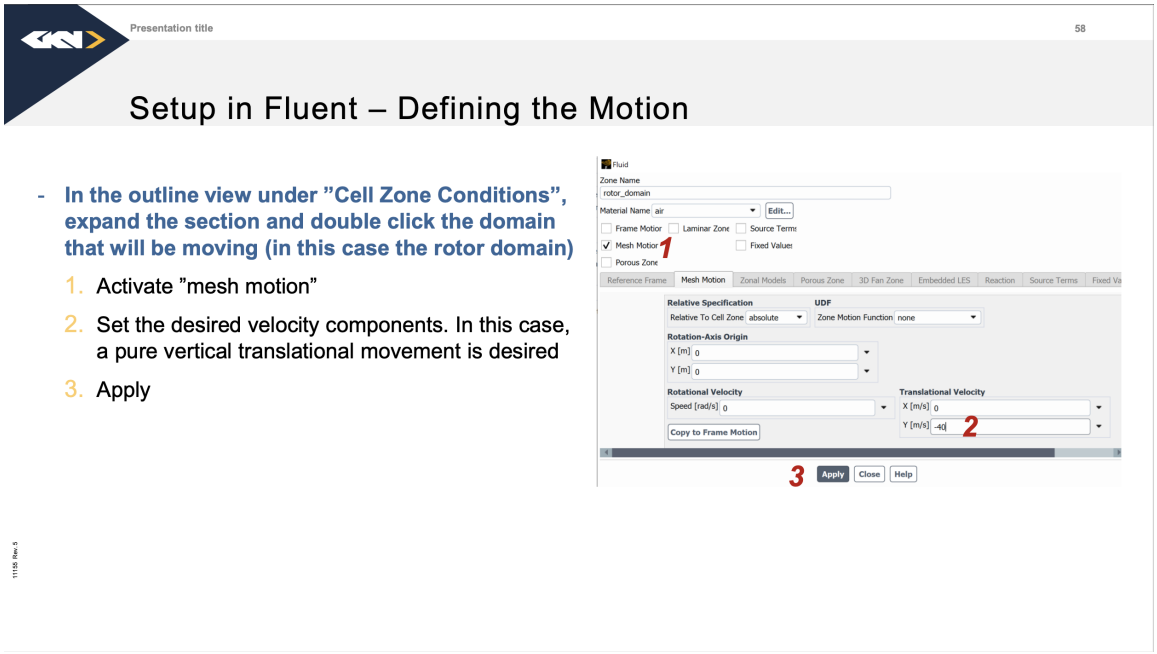

Figure A.7: Sliding mesh guide, part 7/9

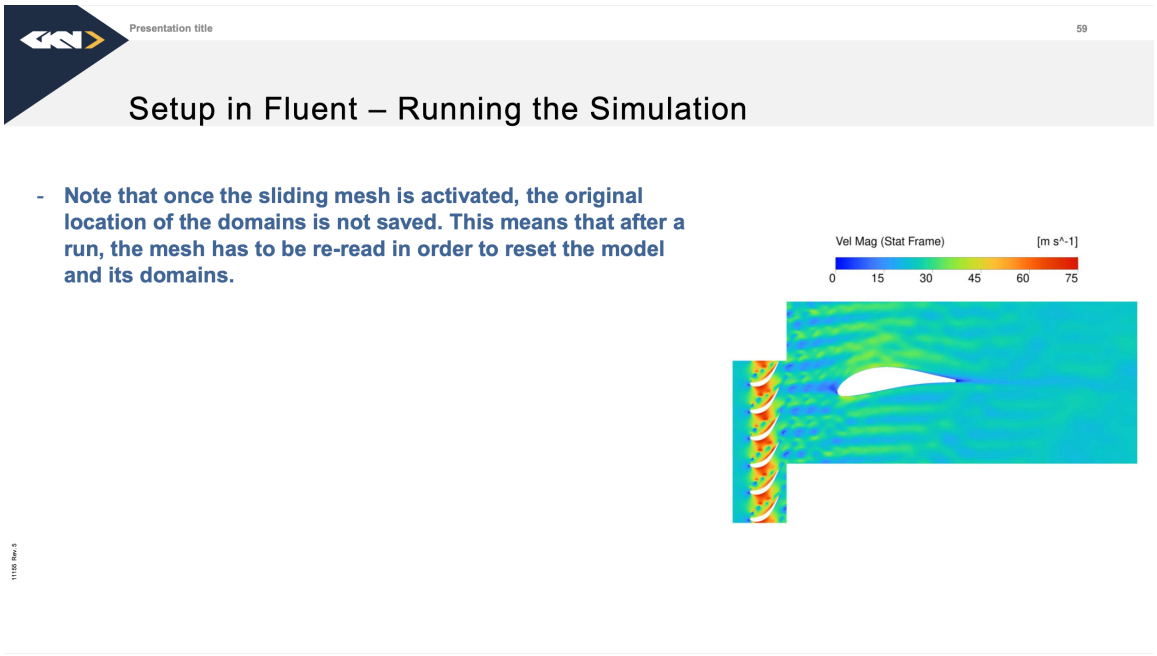

Figure A.8: Sliding mesh guide, part 8/9

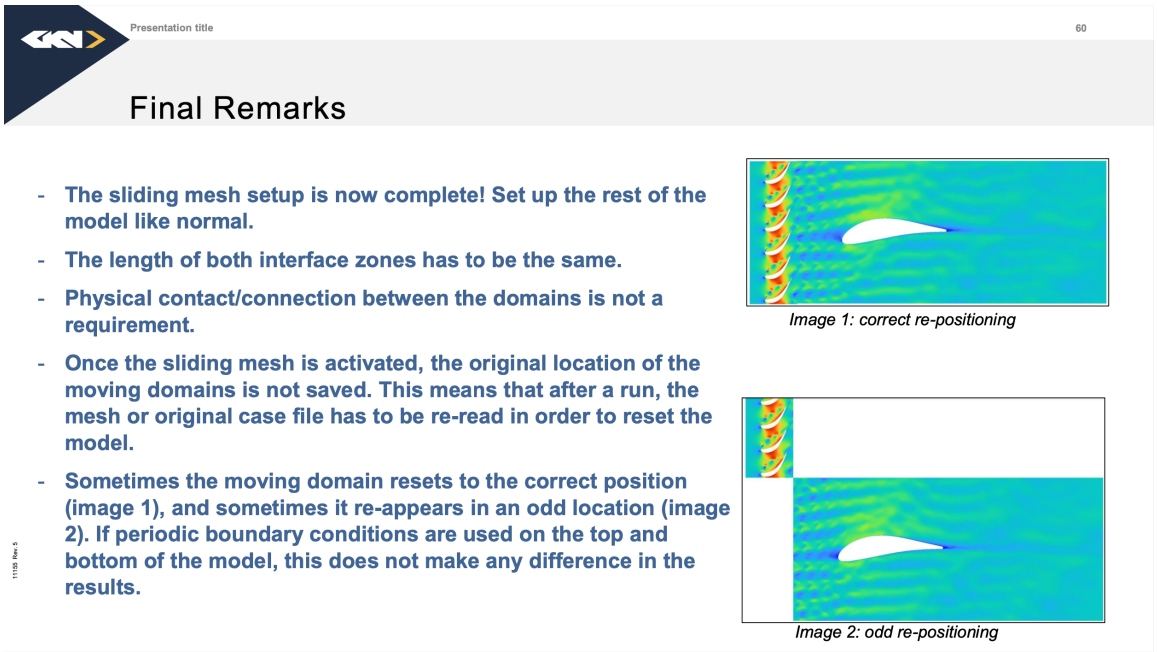

Figure A.9: Sliding mesh guide, part 9/9

A.2 Example of Fluent TUI Script, Transient Case

```
;————————————————————————————————
; final setup, see readme in sims folder for more information.
;————————————————————————————————

;————————— IMPORT MESH —————————;
```

```
file r-c /project/AeroThermo/Exjobb_Wilhelm_Dahlin/cluster_script_sims/
mesh_files_saft_profile/6rotors_1saftvane_le_midspan.msh

;————————- DEFINE TRANSIENT SOLVER ————————;

define models unsteady-2-order y

;————————- SELECT MODELS ————————;

def mod energy y n n n y ;activate energy model
def mod visc trans-sst y ;choose turbulence model
def materials c-c air air y ideal-gas n n n n n n ;change air properties

;————————- MESH MOTION CONDITIONS ————————;

def b-c fluid turbine_domain_fluid n n n n n 0 n 0 n n n n
def b-c fluid ogv_domain_fluid n n n n n 0 n 0 n n n n

;————————- BOUNDARY CONDITIONS ————————;

;set "normal" bcs
def b-c z-t inlet pres-in
def b-c pres-in inlet y n 104000 n 0 n 302.15 y n 1 n -1.5 y n 1 n 1.547 n 5195 y
def b-c pres-out outlet y n 101325 n 302.15 n n y y n 1 n 1.547 n 5195 y y n n
def b-c wall turbine n 0 n 0 y al n n 0 n n n 0 n 0.5 n 1 ;adiabatic
def b-c wall ogv n 0 n 0 y al y temp n 292.15 n n n 0 n 0.5 n 1

;set periodic bcs for each top/bottom pair
def b-c m-z create-periodic-int auto periodic_turbine bottom-turbine_domain_fluid top-
turbine_domain_fluid n y y

def b-c m-z create-periodic-int auto periodic_ogv bottom-ogv_domain_fluid top-ogv_domain_fluid
n y y

;————————- INTERFACE SETUP ————————;

;set interface bc and enable periodic repeats interface
def mesh-int o-t-o-p n y ;enable periodic repeats option

;create the interface
def mesh-int create interface_01 (interface_turbine_edge) (interface_ogv_edge) n y n

;set operating pressure to 0
def op-cond op-pres 0

;————————- REFERENCE VALUES ————————;
```

```
report ref-val zone
turbine_domain_fluid
report ref-val area 0.24
report ref-val density 1.176655
report ref-val depth 1
report ref-val enthalpy 0
report ref-val length 0.2
report ref-val pressure 101325
report ref-val temperature 302.15
report ref-val velocity 43
report ref-val viscosity 1.7894e-05

;————————- SOLVER SETTINGS ————————;

;residual reqs, set to extremely low to prevent it from stopping simulation
solve monitors residual conv-crit 1e-9 1e-9 1e-9 1e-9 1e-9 1e-9 1e-9 1e-9

;coupling settings solve set p-v-c 20 ;(20=simple, 21=simplec, 22=piso, 23=coupled)

;under-relaxation factors
solve set under-relaxation pressure 0.3
solve set under-relaxation density 0.8
solve set under-relaxation body-force 0.7
solve set under-relaxation mom 0.7
solve set under-relaxation k 0.7
solve set under-relaxation omega 0.7
solve set under-relaxation intermit 0.7
solve set under-relaxation retheta 0.7
solve set under-relaxation turb-viscosity 0.6
solve set under-relaxation temperature 0.6

;————————- FILES AND REPORTS ————————;

;autosave case and data files
file auto-save append-file-name-with time-step 6
file auto-save case-freq if-case-is-modified
file auto-save data-freq 1000
file auto-save save-data-file-every time-step
file auto-save retain-most-recent-files y
file auto-save max-files 10000
file auto-save root-name /project/nobackup/AeroThermo/yy56946_temp/sims/transient
/1p5_stage_model_BCs/on_design/sim_stator_BCs/fluent_files/fluentData

solve report-def add inlet-vel surface-areaavg
surface-names (inlet)
field vel-mag q
```

solve report-files add vel-inlet-file report-defs (flow-time inlet-vel) file-name /project /nobackup/AeroThermo/yy56946_temp/sims/transient/1p5_stage_model_BCs/on_design /sim_stator_BCs/report_files/avg_inlet_vel q

;————————- ACTIVATE MESH MOTION ————————;

def b-c fluid turbine_domain_fluid n n n n n 0 n 0 y -1 n 0 n 0 n -38.6 n 0 n 0 none y n n

;————————- SLIDING SIMULATION 1/2 - NO CDAT FILES ————————;

;initialize and run the sim
solve init hyb-init
solve set transient-controls t-s-s 1e-5
solve d-t-i 40000 10

;————————- SLIDING SIMULATION 2/2 - WITH CDAT FILES ————————;

file trans-export cdat-f-c-p--e /project/nobackup/AeroThermo/yy56946_temp/sims/transient /1p5_stage_model_BCs/on_design/sim_stator_BCs/post_files/postData (turbine_domain_fluid ogv_domain_fluid) pressure total-pressure velocity-magnitude x-velocity y-velocity vorticity-mag cell-convective-courant-number temperature turb-kinetic-energy turb-intensity viscosity-turb viscosity-ratio turb-diss-rate production-of-k y-plus x-coordinate y-coordinate quit y only-on-change cdat-export time-step 20 time-step

; activate time-averaging for certain quantities: solve set data-sampling y 2 n y n n
solve set data-sampling-options add-datasets (ogv) heat-flux q t t t t t 1
solve set data-sampling-options add-datasets (turbine_domain_fluid ogv_domain_fluid) turb-kin-en turb-int turb-diss-rate viscosity viscosity-turb viscosity-ratio total-pressure pressure q t t t t t 1

solve d-t-i 5000 10

;————————- EXIT SIMULATION ————————;

exit yes

DEPARTMENT OF MECHANICS AND MARITIME SCIENCES
CHALMERS UNIVERSITY OF TECHNOLOGY
Gothenburg, Sweden
www.chalmers.se

CHALMERS
UNIVERSITY OF TECHNOLOGY